



# 1 **Satellite Detection of NO<sub>2</sub> Distributions and Comparison with** 2 **Ground-Based Concentrations**

3

4 Summer Acker,<sup>1</sup> Tracey Holloway<sup>1,2</sup> and Monica Harkey<sup>1</sup>

5 <sup>1</sup> Nelson Institute Center for Sustainability and the Global Environment, University of Wisconsin-Madison,  
6 Madison, WI 53705, United States of America

7 <sup>2</sup> Department of Atmospheric and Oceanic Sciences, University of Wisconsin-Madison, Madison, WI 53705, United  
8 States of America

9

10 *Correspondence to:* Tracey Holloway ([taholloway@wisc.edu](mailto:taholloway@wisc.edu))

11

## 12 **Abstract**

13 In this study we assess the capability of current-generation satellites to capture the variability of  
14 near-surface nitrogen dioxide (NO<sub>2</sub>) monitoring data, with the goal of supporting health and  
15 regulatory applications. We consider NO<sub>2</sub> vertical column densities (VCD) over the United  
16 States from two satellite instruments, the Tropospheric Monitoring Instrument (TROPOMI), and  
17 Tropospheric Emissions: Monitoring of Pollution (TEMPO), and compare with ground-based  
18 concentrations as measured by the EPA's Air Quality System (AQS) monitors. While  
19 TROPOMI provides a longer-term record of assessment (2019-2023), TEMPO informs diurnal  
20 patterns relevant to evaluating peak NO<sub>2</sub>. We analyze frequency distributions and quantify their  
21 similarity using the Jensen-Shannon Divergence (JSD), where smaller values indicate better  
22 agreement. Satellite and ground monitor NO<sub>2</sub> distributions are most similar away from major  
23 roads, as indicated by the JSD of 0.008 calculated for TROPOMI and ground monitors at non-  
24 roadways, compared with a JSD near interstates of 0.158 and a JSD near highways of 0.095.  
25 Seasonal analysis shows the most similarity in distributions in winter, with a JSD of 0.010, and  
26 the most difference in summer, with a JSD of 0.035. Across seasons and monitor locations,  
27 TEMPO consistently has a lower or similar JSD as TROPOMI, with TEMPO JSDs ranging from  
28 0.005 to 0.151 and TROPOMI JSDs ranging from 0.012 to 0.265. TEMPO's agreement with



29 monitors in both December 2023 and July 2024 is found to be best around midday, with non-  
30 road monitors' JSD in July as low as 0.008 at 16 UTC (~11am LT).

## 31 **1 Introduction**

32 The frequency distribution of ambient pollutants in urban areas has long been recognized as a  
33 useful metric for comparison with health-based thresholds, and to assess the effectiveness of  
34 emission controls. Early studies found pollutant concentrations in urban areas to be  
35 approximately lognormally distributed (Knox and Lange, 1974; Pollack, 1975; Venkatram,  
36 1979) and isolated point sources better described by exponential distributions (Venkatram,  
37 1979). The distributional lens also bears relevance to advanced health and regulatory assessment  
38 (Chowdhury et al., 2021; Mondal et al., 2021). In this study we evaluate the capability of current-  
39 generation satellites to capture the variability of near-surface nitrogen dioxide (NO<sub>2</sub>) monitoring  
40 data, with the goal of supporting health and regulatory applications.

41 Nitrogen dioxide (NO<sub>2</sub>) is a gas released through high temperature combustion processes such as  
42 the burning of fossil fuels (Lee et al., 1997; Richter et al., 2005), with on-road vehicles, power  
43 plants, and industrial processes representing the largest anthropogenic sources in the United  
44 States (U.S.; van der A et al., 2008). Exposure to elevated levels of NO<sub>2</sub> has been linked to  
45 respiratory and cardiovascular diseases (Mills et al., 2015; Urbanowicz et al., 2023; Meng et al.,  
46 2021), especially asthma in children (Mölter et al., 2014; Anenberg et al., 2022; Achakulwisut  
47 et al., 2019), as well as premature mortality (Camilleri et al., 2023; Hales et al., 2021; Huangfu and  
48 Atkinson, 2020), and other diseases (Xia et al., 2024; Bai et al., 2018). NO<sub>2</sub> plays a critical role  
49 in the formation of ozone, which also causes respiratory health problems and is harmful to  
50 ecosystems (Grulke & Heath, 2019; Sillman, 1999). It is also a precursor to nitrate (Behera &  
51 Sharma, 2012), a type of fine particulate matter (PM<sub>2.5</sub>), which can penetrate deep into the lungs  
52 and exacerbate respiratory and heart conditions (Sangkham et al., 2024; Sharma et al., 2020), as  
53 well as cause premature death (Orellano et al., 2020; Thangavel et al., 2022).

54 The EPA Air Quality System (AQS) contains hourly NO<sub>2</sub> measurements from ground-based  
55 monitors, providing high temporal resolution data that are critical for assessing compliance with  
56 the U.S. National Ambient Air Quality Standards (NAAQS). There are two NAAQS related to  
57 NO<sub>2</sub>: one for annual average concentration, set at 53 ppb, and one based on peak 1-hour



58 concentrations, set at 100 ppb, based on the 3-year average of the 98<sup>th</sup> percentile of the yearly  
59 distribution of 1-hour daily maximum NO<sub>2</sub> concentrations (EPA, 2010). Enforcement of these  
60 standards relies on data from AQS NO<sub>2</sub> monitors, a network that includes 431 monitors as of  
61 2024. Because NO<sub>2</sub> has a relatively short atmospheric lifetime, typically ranging from a few  
62 hours to a day depending on meteorological conditions (Lange et al., 2022; Liu et al., 2021),  
63 ground monitors are expected to capture local conditions (Wang et al., 2020).

64 Several studies have highlighted the potential for satellite NO<sub>2</sub> data to supplement ground-based  
65 networks (Duncan et al., 2014; Lee & Koutrakis, 2014). Due to its radiative characteristics, NO<sub>2</sub>  
66 may be observed by satellites during daylight hours (Boersma et al., 2018; Van Geffen et al.,  
67 2020; Veeffkind et al., 2012), and NO<sub>2</sub> has emerged as one of the most air-quality-relevant  
68 pollutants from satellites (Holloway et al., 2021). Some of the first studies done comparing  
69 ground-based NO<sub>2</sub> to satellite VCDs (Lamsal et al., 2014; Lamsal et al., 2015; Zhang et al.,  
70 2018) used the Ozone Monitoring Instrument (OMI, 13 km × 24 km; Levelt et al., 2006). Annual  
71 OMI and surface NO<sub>2</sub> trends in the U.S. show that OMI usually overestimates the surface trends  
72 by ~3.7% each year (Zhang et al., 2018). With the 2017 launch of the Tropospheric Monitoring  
73 Instrument (TROPOMI; Boersma et al., 2018; Van Geffen et al., 2020; Veeffkind et al., 2012),  
74 new opportunities arose for analyzing column-to-surface agreement at a higher resolution (3.5  
75 km x 5.5 km) (Goldberg et al., 2021; Griffin et al., 2019; Kim et al., 2024; Yu & Li, 2022;  
76 Dressel et al., 2022; Goldberg et al., 2024; H. J. Lee et al., 2023).

77 While advanced methods exist to calculate near-surface NO<sub>2</sub> explicitly (Ahmad et al., 2024; Kim  
78 et al., 2021; Shetty et al., 2024; Virta et al., 2023), there is also a strong interest in the utilization  
79 of satellite vertical column density (VCD) to directly infer NO<sub>2</sub> concentrations analogous to  
80 ground-based monitors (Kim et al., 2024; Lamsal et al., 2014; Griffin et al., 2019; Yu & Li,  
81 2022; Zhang et al., 2018; Lamsal et al., 2015; Goldberg et al., 2021; Dressel et al., 2022;  
82 Goldberg et al., 2024; Harkey & Holloway, 2024; Bechle et al., 2013; H. J. Lee et al., 2023; Xu  
83 & Xiang, 2023). This study extends these prior assessments of NO<sub>2</sub> column-to-surface  
84 agreement, where we focus on frequency distributions to capture the net impact of day-to-day  
85 variability.



86 Past studies comparing surface and satellite NO<sub>2</sub> have found temporal correlation of daily values  
87 at individual sites ranging from  $r=0.61$  to  $r=0.69$  (Lamsal et al., 2014; Lamsal et al., 2015),  
88 monthly and seasonal values at individual sites ranging from  $r=0.67$  to  $r=0.90$  (Griffin et al.,  
89 2019; Yu & Li, 2022; Harkey & Holloway, 2024; Dressel et al., 2022; Xu & Xiang, 2023;  
90 Lamsal et al., 2015), and annual average values at sites ranging from  $r=0.68$  to  $r=0.93$  (Zhang et  
91 al., 2018; Lamsal et al., 2015; Goldberg et al., 2021; Kim et al., 2024; Bechle et al., 2013; H. J.  
92 Lee et al., 2023). Here,  $r$  refers to the Pearson correlation coefficient, which measures the  
93 strength and direction of a linear relationship between variables. In some cases, these  
94 comparisons adjusted column values to the surface (e.g. Lamsal et al., 2014) and/or adjusted  
95 ground-monitors to reduce the error in chemiluminescent detection of NO<sub>2</sub> (e.g. Lamsal et al.,  
96 2015; Bechle et al., 2013). Using similar methods, TROPOMI tends to show better agreement  
97 with annual AQS NO<sub>2</sub> than does OMI, e.g.  $r=0.81$  using TROPOMI (Goldberg et al., 2015)  
98 versus  $r=0.68$  from OMI (Lamsal et al., 2015). Off-road AQS monitors tend to show better  
99 agreement with satellite data than near-road AQS monitors, e.g.  $r = 0.81-0.87$  at non-near-road  
100 sites versus  $r = 0.64-0.74$  at near-road sites (Kim et al., 2024). The underestimation of estimated  
101 near-surface NO<sub>2</sub> near roads and localized sources is a recurring issue in OMI and TROPOMI  
102 NO<sub>2</sub> VCDs (Dressel et al., 2022; Goldberg et al., 2024; Ialongo et al., 2020).

103 The relationship between surface NO<sub>2</sub> and column abundance is influenced by physical and  
104 chemical processes, many of which have seasonal components. In winter, shallow boundary  
105 layers trap pollutants near the surface, leading to higher surface concentrations and increasing  
106 surface-to-column agreement (Harkey et al., 2015). In summer, higher temperatures and  
107 increased sunlight accelerate photochemical reactions, converting NO<sub>2</sub> into ozone and other  
108 secondary pollutants, and decreasing surface-to-column agreement (Boersma et al., 2009).  
109 Seasonal changes in emissions, such as high building-heating emissions in winter, and high  
110 power plant emissions in summer (Frost et al., 2006; Levinson & Akbari, 2010) interact with  
111 atmospheric processes causing an increase in NO<sub>2</sub> column abundance in winter in four-season  
112 climates (Shah et al., 2020). Processes affecting the sources and sinks of NO<sub>2</sub> at the surface and  
113 through the vertical column can also lead to temporal lags, with peak surface NO<sub>2</sub> preceding  
114 peak column NO<sub>2</sub> in the mornings (Harkey et al. 2024).



115 Frequency distributions capture the variability, extremes, and patterns of pollutant abundance,  
116 relevant to air quality standards, pollution trends, and the effectiveness of emission control  
117 measures. For example, Mondal et al. (2021) used frequency distributions of ground-based  
118 monitors to examine changes in air quality across Delhi and Kolkata during COVID-19  
119 lockdown phases, showing how reduced human activity led to shifts in pollutant levels. We  
120 extend this line of analysis by comparing NO<sub>2</sub> distributions across multiple dimensions with  
121 TROPOMI and include time-of-day and resolution-dependence of results using data from the  
122 Tropospheric Emissions: Monitoring of Pollution (TEMPO; Chance et al., 2019; Naeger et al.,  
123 2021; Zoogman et al., 2017). TEMPO provides daytime hourly observations of NO<sub>2</sub> over North  
124 America and finer spatial coverage—approximately 2.1 km by 4.5 km at its center.

125 The Jensen-Shannon Divergence (JSD) is a robust metric for comparing probability distributions  
126 that is used within a wide variety of fields, including machine learning (Thiagarajan & Ghosh,  
127 2024; Saurette et al., 2023; Tsigalou et al., 2021; Melville et al., 2005), data science (Toledo et  
128 al., 2022; Zhao et al., 2024), biology (Yan et al., 2021; Jones et al., 2023; Ahmed et al., 2023),  
129 and meteorology (Kibirige et al., 2023). In environmental research using satellite data, the JSD  
130 has shown that the Mangrove Forest Index (MFI) from Sentinel-2 imagery outperforms  
131 traditional vegetation indices in distinguishing submerged mangrove forests (Jia et al., 2019). In  
132 air quality, JSD has been used to compare modeled and measured PM<sub>2.5</sub> (Yang et al., 2024), and  
133 to compare an air quality index (AQI) with measurements of specific air pollutants (Wang &  
134 Zhang, 2022). We utilize the JSD to quantify the similarity between satellite and monitored NO<sub>2</sub>  
135 distributions, applying this well-established metric to satellite-derived air quality evaluation.

136 In this work, we consider: (1) How do the distributions of satellite NO<sub>2</sub> VCD compare with those  
137 for near-surface NO<sub>2</sub>? (2) To what degree does new hourly data from TEMPO improve the  
138 agreement between surface and space based NO<sub>2</sub> distributions? For both questions, we consider  
139 spatial variability, especially proximity to roadways, and temporal variability including  
140 seasonality and diurnal variability. By considering the ability of satellites to capture peak NO<sub>2</sub>  
141 values in a comparable distribution to surface data, we consider how satellite VCDs can support  
142 air quality management, improve health impact analysis, and inform air pollution monitor siting.



## 143 **2 Data and Methods**

144 In this study, we evaluate the ability of two satellite instruments, TROPOMI and TEMPO, to  
145 capture the spatial and temporal variability in NO<sub>2</sub> surface concentration distributions across the  
146 continental United States (CONUS), as measured by AQS monitors. By comparing the  
147 coefficient of variation (CV) and Jensen-Shannon divergence (JSD) between satellite and  
148 monitor data, we aim to assess the alignment between the datasets.

### 149 **2.1 EPA Surface Monitor Data**

150 The EPA Air Quality System (AQS) was used to access NO<sub>2</sub> monitor data for the years 2019  
151 through 2023 from all available sites in CONUS during this time period (N=503). Most monitors  
152 use a chemiluminescence method, where the amount of NO<sub>2</sub> that is converted to NO is measured  
153 by a molybdenum oxide converter (Fontijn et al., 1970). The converter also reacts with other  
154 oxidized nitrogen compounds such as nitric acid (HNO<sub>3</sub>) and peroxyacetyl nitrate (PAN) to form  
155 NO (Dunlea et al., 2007; Steinbacher et al., 2007), which can lead to an overestimation of NO<sub>2</sub>.  
156 Corrections for this bias have been applied when comparing with satellite observations (e.g.  
157 Cooper et al., 2020; Lamsal et al., 2015; Li et al., 2021). Uncorrected AQS NO<sub>2</sub> has been used  
158 for determining compliance with the NAAQS and for health assessments, which is the approach  
159 we take here, consistent with prior studies focused on regulatory relevance (Novotny et al., 2011;  
160 Penn & Holloway, 2020; Harkey and Holloway, 2024; Goldberg et al., 2021; Kim et al., 2024;  
161 Duncan et al., 2013; Qin et al., 2019). More recently, some NO<sub>2</sub> monitors have been added to the  
162 network which measure “true NO<sub>2</sub>” using Cavity Attenuated Phase Shift Spectroscopy (CAPS,  
163 Keabian et al., 2005). These monitors are expected to be more representative of ground-level  
164 NO<sub>2</sub> concentrations and have less overestimations since they directly measure NO<sub>2</sub> and no other  
165 species (Ge et al., 2013). Some of the monitors used in this study use CAPS methodology to  
166 measure NO<sub>2</sub>. We discuss the comparison of CAPS versus traditional NO<sub>2</sub> monitors in results  
167 Sect. 3.1.

168 Hourly AQS measurements at 13:00 and 14:00 local time (LT) were averaged to align with the  
169 TROPOMI overpass of ~13:30 LT. Hourly AQS measurements from 12:00 GMT to 23:00 GMT  
170 are compared with hourly TEMPO data for daylight hours. For both the TROPOMI and TEMPO  
171 analyses, AQS data are filtered to ensure consistency with satellite data availability. As a result



172 of filtering monitoring data for TROPOMI and TEMPO separately, the subsets of monitor data  
173 available for comparison with each instrument differ, even for the same time periods.

## 174 **2.2 TROPOMI Data**

175 The Tropospheric Monitoring Instrument (TROPOMI) is on board the Copernicus Sentinel-5  
176 Precursor satellite which has a daily, local overpass time of ~13:30 LST (Veefkind et al., 2012).  
177 Currently, the highest resolution of TROPOMI is 3.5 km by 5.5 km at nadir which has increased  
178 from 3.5 km by 7.0 km since August 6<sup>th</sup>, 2019. Daily TROPOMI NO<sub>2</sub> data for the years 2019  
179 through 2023 were allocated to a 4 km x 4 km grid over CONUS using the Wisconsin Horizontal  
180 Interpolation Program for Satellites (WHIPS; Harkey et al., 2015, 2021; Harkey and Holloway,  
181 2024; Penn and Holloway, 2020). Using WHIPS, we also remove data with quality flag lower  
182 than 0.75. Each monitor location was compared with the 4 km x 4 km gridded TROPOMI value  
183 in the corresponding grid cell. December 2023 and July 2024 4 km x 4 km TROPOMI NO<sub>2</sub> data  
184 were also collected for each of the monitors for comparison with TEMPO data.

## 185 **2.3 TEMPO Data**

186 The TEMPO instrument launched onboard the Intelsat 40e mission (NASA, 2024), a  
187 geostationary satellite, on April 7, 2023. TEMPO provides hourly measurements of atmospheric  
188 pollutants over North America (Chance et al., 2019; Naeger et al., 2021; Zoogman et al., 2017).  
189 TEMPO achieves a spatial resolution of approximately 2.1 km in the north-south direction and  
190 4.5 km in the east-west direction at the center of its Field of Regard (FOR), centered around  
191 36.5° N and 100° W (Chance et al., 2019). The TEMPO Level-3 (L3) NO<sub>2</sub> data (Suleiman, 2024)  
192 used in this study were accessed through NASA's EarthData Search portal.

193 In order to synchronize TEMPO and ground-based hourly measurements, TEMPO timestamps  
194 were rounded to the nearest hour, with mid-hour values rounded up. All files within each  
195 rounded-hour group were averaged, producing a single NO<sub>2</sub> value per hour per day. Only  
196 TEMPO observations with a main data quality flag of 0 and cloud fraction at or less than 0.2  
197 were retained, in line with TEMPO documentation guidelines (NASA Langley Research Center,  
198 2024).



199 For the comparison with TROPOMI, the UTC equivalents of 1 pm and 2 pm LT were  
200 determined for each time zone based on the latitude and longitude of each monitor location.  
201 TEMPO NO<sub>2</sub> values corresponding to these calculated UTC hours were averaged to align with  
202 the TROPOMI overpass time (~13:30 LST). Similarly, for ground-based measurements, the  
203 monitor data were filtered to include only values corresponding to 1 pm and 2 pm LT and then  
204 averaged.

#### 205 **2.4 Monitor Classification**

206 To classify the monitors by roadway proximity, the state-level Census Bureau's 2021  
207 TIGER/Line shapefiles for Primary and Secondary Roads were combined to form a  
208 comprehensive dataset for the CONUS domain.

209 To evaluate how TROPOMI and ground-based monitor NO<sub>2</sub> values vary by proximity to a road,  
210 monitors were also assigned to different groups based on their distance from a road ( $\leq 20$ -m, 20  
211 to 50-m, 50 to 300-m, 300-m to 1mi, and  $>1$ mi), where buffer distances are calculated from the  
212 road shapefiles (Figure S2). There were 9 monitors that were 20 meters or less away from a road,  
213 66 between 20 and 50 meters from a road, 108 between 50 and 300 meters, 219 between 300  
214 meters and 1 mile, and 101 that were greater than 1 mile from a road.

215 Roads were also classified into three categories: (1) interstates, (2) highways, and (3) other  
216 roads, based on their route type code (RTTYP) values. Where monitors are considered as  
217 representing a roadway category, we followed the criteria of the EPA Near-Road-Network  
218 (Gantt et al., 2021; Kim et al., 2024), to merge monitor locations with road buffers, considering  
219 the 50-m buffer recommended by EPA, as well as a less restrictive 300-m buffer. In each case,  
220 monitors inside the buffer of a particular roadway type were classified as representing that  
221 category. If a monitor fell within multiple buffers, it was assigned the classification of the largest  
222 road type. Monitors not falling within any buffers were classified as "non-roadway."

223 Using the 50-m buffer, 58 monitors were classified as "interstate," 17 as "highway," and 428 as  
224 "non-roadway" (Figure S1; no monitors classified as "other roads"). Using the 300-m buffer, 91  
225 monitors were classified as "interstate," 90 as "highway," 320 as "non-roadway," and 2 as "other





226 roads.” Since there were no monitors classified as “other roads” for the 50-m buffer, this  
227 category is excluded from the analysis.

## 228 **2.5 Data Analysis**

229 The coefficient of variation (CV) was calculated for ground-level monitor data and for satellite  
230 data. This metric was used to compare the relative variability of NO<sub>2</sub> between satellite and  
231 ground-level data despite different measurement units (Aerts et al., 2015). CV is defined as the  
232 ratio of the standard deviation ( $\sigma$ ) to the mean ( $\mu$ ) of the data:

$$233 \quad CV = \left( \frac{\sigma}{\mu} \right) \times 100$$

234 The Jensen-Shannon Divergence (JSD) quantifies the similarity between the distributions of NO<sub>2</sub>  
235 from satellite and ground-level monitors despite the different measurement units (Menéndez et  
236 al., 1997). To calculate JSD, each dataset was binned, with a bin size of 1 ppb or  $1 \times 10^{15}$   
237 molecule/cm<sup>2</sup>, ranging from 0 to 40 ppb or  $40 \times 10^{15}$  molecule/cm<sup>2</sup>, with an additional bin for  
238 values exceeding 40 ppb or  $40 \times 10^{15}$  molecule/cm<sup>2</sup>. Binned data were then normalized to form  
239 probability distributions. The divergence was calculated as:

$$240 \quad JSD(P, Q) = \frac{1}{2} [D_{KL}(P||M) + D_{KL}(Q||M)]$$

241 where P and Q represent the probability distributions from the monitor and satellite data,  
242 respectively, and M is the average of P and Q. The divergence  $D_{KL}$  is the Kullback-Leibler  
243 divergence between each distribution and their mean (Clim et al., 2018). JSD values range from  
244 0 to 1, with lower values indicating greater similarity between the satellite and monitor  
245 distributions. In general, a  $JSD < 0.1$  indicates very good alignment,  $0.1 \leq JSD < 0.3$  indicates  
246 moderate alignment, and  $JSD \geq 0.3$  (Kibirige et al., 2023) indicates poor alignment.

## 247 **3 Results**

248 To evaluate the agreement between satellite and monitored NO<sub>2</sub> distributions, we consider the  
249 impact of monitor location using TROPOMI; impact of season using TROPOMI; the comparison  
250 of distributions between TROPOMI and TEMPO; and the impact of time-of-day using TEMPO.



### 251 3.1 Alignment of TROPOMI NO<sub>2</sub> Distributions with Surface NO<sub>2</sub> Distributions

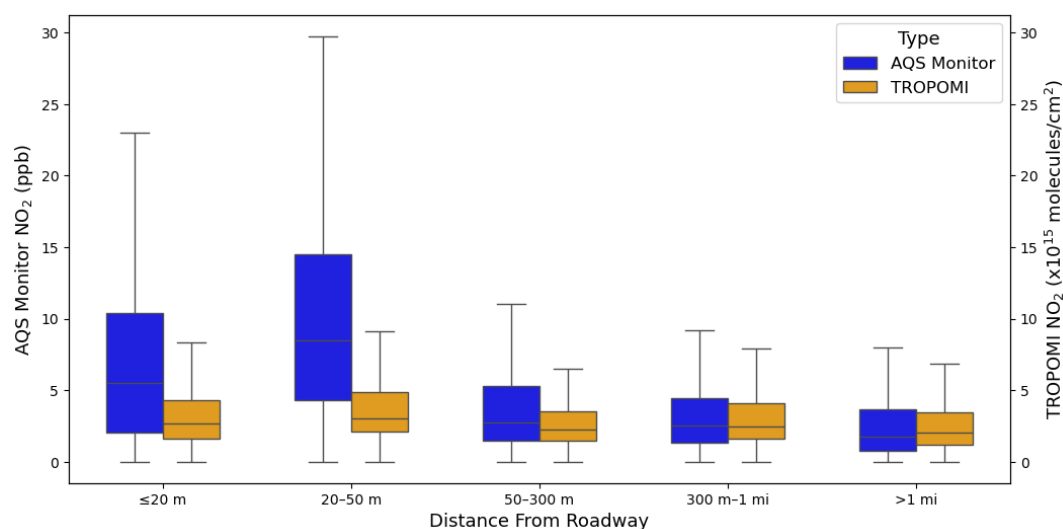
252 Figure 1 illustrates the distribution of NO<sub>2</sub> levels measured by AQS ground-based monitors and  
253 TROPOMI observations as a function of distance from roadways. For both data sources, mean,  
254 peak, and minimum NO<sub>2</sub> are all highest in the 20 – 50m distance category (the second closest  
255 near-road category). NO<sub>2</sub> abundance decreases as distance-to-road increases, and to a lesser  
256 extent as distance-to-road decreases. The somewhat lower abundance  $\leq 20$  m vs. the 20 – 50 m  
257 category may be due to the speciation of NO<sub>x</sub>, where NO is more abundant and converts to a  
258 higher fraction of NO<sub>2</sub> as distance-to-road increases (Kimbrough et al., 2017). Mean monitored  
259 NO<sub>2</sub> is 6.85 ppb at  $\leq 20$  m, 10.47 ppb at 20 – 50 m, 4.53 ppb at 50 – 300 m, 3.53 ppb at 300 m –  
260 1 mi, and 2.76 ppb at  $> 1$  mi. Mean TROPOMI NO<sub>2</sub> is  $3.38 \times 10^{15}$  molecules/cm<sup>2</sup> at  $\leq 20$  m,  $4.21$   
261  $10^{15}$  molecules/cm<sup>2</sup> at 20 – 50 m,  $3.00 \times 10^{15}$  molecules/cm<sup>2</sup> at 50 – 300 m,  $3.63 \times 10^{15}$   
262 molecules/cm<sup>2</sup> at 300 m – 1 mi, and  $3.04 \times 10^{15}$  molecules/cm<sup>2</sup> at  $> 1$  mi. Monitor values show a  
263 higher sensitivity to roadway proximity, where the highest mean monitored concentration is  
264 379% of the lowest mean concentration, compared to TROPOMI where the highest mean VCD  
265 is 138% of the lowest mean VCD.

266 Monitored NO<sub>2</sub> levels drop over 50% at  $\sim 50$  m from the roadway (based on change in the mean,  
267 upper 2.5 interquartile range, IQR, and the upper 1.5 IQR), a finding that compares with 31%  
268 reduction in NO<sub>2</sub> between 20m and 300m from Kimbrough et al. (2017), as well as other studies  
269 that identify a decrease in NO<sub>2</sub> at further distances (Karner et al., 2010; Richmond-Bryant et al.,  
270 2017). TROPOMI VCDs also show the greatest change with roadway distance at  $\sim 50$  km, but by  
271 less than 30% (based on change in the mean, upper 2.5 IQR, and the upper 1.5 IQR).

272 Just as total NO<sub>2</sub> abundance, from both monitors and satellite, is highest at distances of 20-50 m  
273 from the roadway, the range of daily values is also widest for the 20 – 50 m range and smallest at  
274 the  $> 1$  mi range. Monitored values have a standard deviation of 8.24 ppb in the 20 – 50 m range,  
275 and a standard deviation of 3.44 ppb in the  $> 1$  mi range. The distribution of satellite data does  
276 not vary as much in size across roadway locations, with a standard deviation of  $3.90 \times 10^{15}$   
277 molecules/cm<sup>2</sup> for the 20 – 50 m range and  $3.39 \times 10^{15}$  molecules/cm<sup>2</sup> for the  $> 1$  mile range. In  
278 the 20 – 50 m range, the upper IQR of AQS NO<sub>2</sub> is 38% higher than the mean. TROPOMI shows  
279 less variability than the monitors, with the 20 – 50 m upper IQR 16% higher than the mean. As  
280 distance from the roadway increases, the distributions of data from ground and satellite become



281 more comparable. In the > 1 mile range, the upper IQR of monitor NO<sub>2</sub> is 30% higher than the  
282 mean and the upper IQR of satellite data is 15% higher than the mean. The ranges show more  
283 similarity at greater distance from the roadway, but even at distances of > 1 mile, the range of  
284 monitored values exceeds the range of satellite VCDs. These patterns agree with Kim et al.  
285 (2024), who found that surface monitors show better agreement with TROPOMI further from  
286 major roads.



287

288 Figure 1. Box plots show median and interquartile ranges of NO<sub>2</sub> as measured by AQS monitors  
289 (blue) and TROPOMI (orange) across various distances from roadways, with the whiskers  
290 extending to the 1.5 IQR range. No outliers are shown. The left y-axis represents AQS monitor  
291 values in parts per billion (ppb), and the right y-axis represents TROPOMI NO<sub>2</sub> values in 10<sup>15</sup>  
292 molecules per cm<sup>2</sup>. The distance categories from the roadway include ≤20m, 20-50m, 50-300m,  
293 300m-1mi, and >1mi.

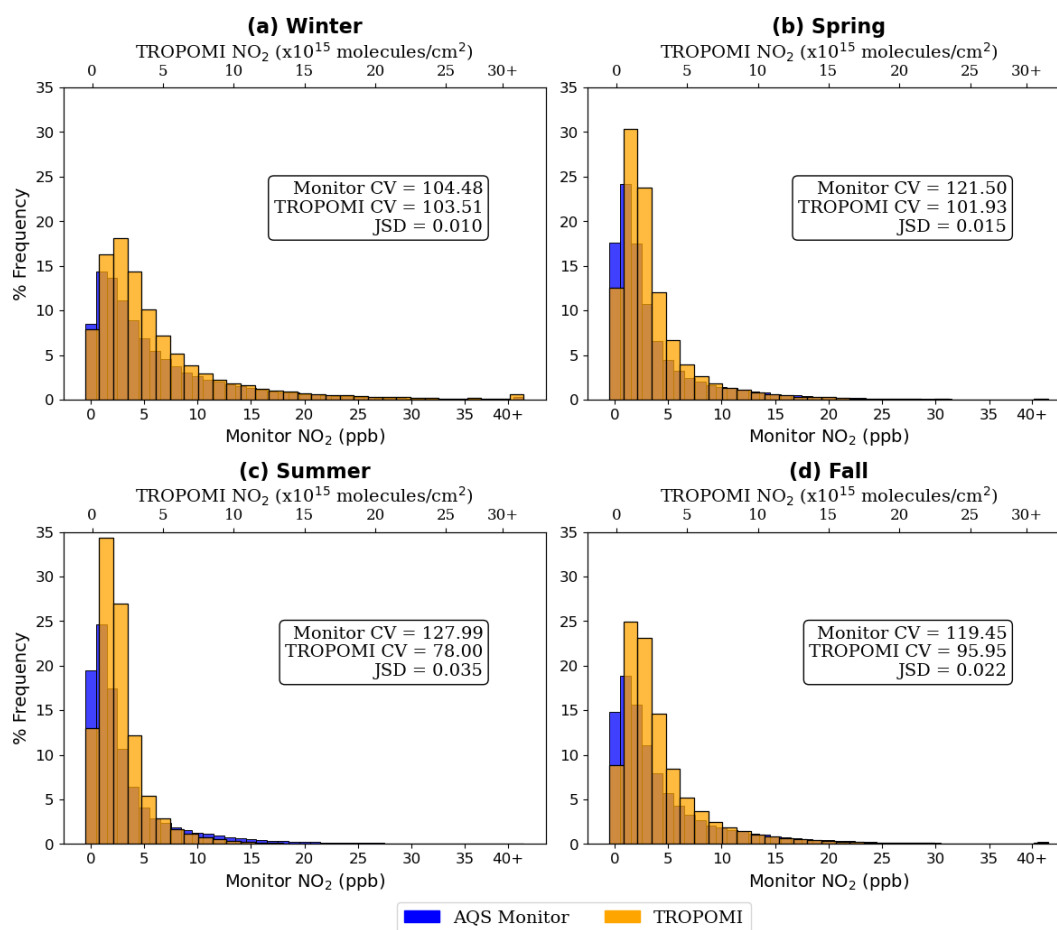
294 To consider the shape of monitored and satellite NO<sub>2</sub> distributions, we consider the effect of  
295 season in Fig. 2. The winter distributions (Figure 2a, calculated from December, January, and  
296 February data) exhibit the longest tails and highest NO<sub>2</sub> values. In winter the 90<sup>th</sup> percentile of  
297 monitoring data is 14.80 ppb and the 90<sup>th</sup> percentile of TROPOMI data is 10.93 x 10<sup>15</sup>  
298 molecules/cm<sup>2</sup>. In summer (Figure 2c, June, July, and August) the distributions exhibit the  
299 shortest tails, and the lowest NO<sub>2</sub> values (90<sup>th</sup> percentile from monitors = 9.00 ppb, 90<sup>th</sup>



300 percentile from TROPOMI =  $4.57 \times 10^{15}$  molecules/cm<sup>2</sup>). The fall (Figure 2d, September,  
301 October, and November) and spring (Figure 2b, March, April, and May) distributions show  
302 behavior in between winter and summer. The higher NO<sub>2</sub> values in winter from monitor and  
303 TROPOMI data are attributed to reduced photochemical activity in winter leading to longer NO<sub>2</sub>  
304 lifetimes (Harkey et al., 2015; Boersma et al., 2009; Shah et al., 2020).

305 The highest percent frequencies for the monitor and TROPOMI distributions generally occur  
306 within the 1–2 ppb or  $1-2 \times 10^{15}$  molecules/cm<sup>2</sup> bin. However, the winter TROPOMI distribution  
307 peaks in the  $2-3 \times 10^{15}$  molecules/cm<sup>2</sup> bin with a percent frequency of 18.14%, compared with  
308 winter monitor highest frequency of 14.33%. The highest percent frequency in spring from  
309 TROPOMI is 30.39% versus monitor 24.15%; in summer TROPOMI is 34.35% versus monitor  
310 of 24.68%; in fall TROPOMI is 24.90% versus monitor of 18.89%. These results indicate that  
311 TROPOMI consistently records higher peak frequencies than the monitors, whereas monitors  
312 consistently show a wider distribution.

313 Figure 2 provides a seasonal breakdown of the coefficient of variation (CV) and Jensen-Shannon  
314 divergence (JSD) for both monitor and TROPOMI data across all monitors. Summer exhibits the  
315 highest variability in monitored NO<sub>2</sub> concentrations (CV = 127.99%), but the lowest variability  
316 in satellite observations (CV = 78.00%). The highest variability in TROPOMI occurs in winter  
317 (CV = 103.51%), similar to the variability from monitor data (CV = 104.48%). Satellite CVs  
318 generally follow a similar pattern to that of the monitors, though the overall variability is lower  
319 for satellite data across seasons.



320

321 Figure 2. Seasonal frequency distributions of 2019-2023 NO<sub>2</sub> as measured by AQS ground-based  
322 monitors (blue) and TROPOMI (light orange) data for four seasons: a) winter, b) spring, c)  
323 summer, and c) fall. The x-axes indicate the range of NO<sub>2</sub>, with the primary, lower x-axis  
324 showing monitor NO<sub>2</sub> concentrations in parts per billion (ppb) and the secondary, upper x-axis  
325 showing TROPOMI NO<sub>2</sub> VCD in 10<sup>15</sup> molecules per cm<sup>2</sup>. The boxes show the Coefficient of  
326 Variation (CV; %) and Jensen Shannon Divergence (JSD) for each season.

327 This reduced variability in satellite observations can likely be attributed to the vertical mixing  
328 reflected in satellite retrievals, as well as horizontal spatial averaging reflected in satellite data  
329 versus point-based NO<sub>2</sub> that are captured by ground monitors. This finding is consistent with  
330 previous studies that highlight the spatial averaging nature of satellite-based measurements,



331 which integrate NO<sub>2</sub> amounts over a larger area than the point-based monitors (Ialongo et al.,  
332 2020).

333 Across all seasons shown in Fig. 2, JSD values are all low ( $< 0.1$ ), indicating that TROPOMI  
334 may be good at predicting surface NO<sub>2</sub> across seasons. The alignment is strongest in winter (JSD  
335 = 0.010), while the divergence is highest in summer (JSD = 0.035), meaning the monitors and  
336 TROPOMI align best when the NO<sub>2</sub> lifetime is long in the colder months, and align the worst  
337 when the NO<sub>2</sub> lifetime is short in the warmer months.

338 Across seasons, we find that CAPS or “true NO<sub>2</sub>” monitors tend to have slightly worse alignment  
339 with TROPOMI than traditional, chemiluminescence monitors. Out of the monitors used in this  
340 study, 102 were identified as CAPS monitors, and 401 as traditional monitors. In winter, CAPS  
341 monitors have a JSD of 0.027 and traditional monitors a JSD of 0.009. In summer, CAPS  
342 monitors have a JSD of 0.078 and traditional monitors a JSD of 0.03. With all seasons combined,  
343 CAPS monitors have a JSD of 0.047 and traditional monitors have a JSD of 0.016.

344 Table 1 shows the CV and JSD for both monitor and satellite data from 2019 through 2023,  
345 aggregated across all seasons and separated by monitor classification (interstate, highway, and  
346 non-roadway), where roadway monitors are classified as being within 50 meters (Table 1a) or  
347 300 meters (Table 1b) of a road. For the 50-m buffer (Table 1a), the coefficient of variation for  
348 ground-based monitor data increases progressively from interstate monitor locations to non-  
349 roadway locations, with interstate monitors exhibiting the lowest variability (CV = 75.07%) and  
350 non-roadway monitors showing the highest variability (CV = 118.17%). This indicates that NO<sub>2</sub>  
351 concentrations measured by ground monitors in interstate areas are more consistent compared to  
352 non-roadway regions. This pattern is mirrored in the satellite data, with CV values ranging from  
353 91.62% for highway monitors to 106.16% for non-roadway monitors. These patterns suggest that  
354 regular emissions play a larger role in determining near-road NO<sub>2</sub>, where non-road areas vary  
355 with changes in wind patterns and the chemical environment.

356 For highway monitors, the CVs of satellite (CV = 91.62%) and monitor data (CV = 96.27%) are  
357 similar, indicating that TROPOMI performs similarly to ground monitors in capturing NO<sub>2</sub>  
358 variability along highways. Near interstates, TROPOMI (CV = 92.60%) may capture more  
359 variability than the ground-based measurements (CV = 75.07%), a finding that contrasts with  
360 Fig. 1, where TROPOMI shows a narrower range of NO<sub>2</sub> values across all distances. This



361 difference could stem from the fact that the interquartile ranges in Fig. 1 measure the spread of  
 362 absolute values, while the coefficient of variation accounts for variability relative to the mean.  
 363 Together, these metrics reveal that TROPOMI may not fully capture localized extremes  
 364 (narrower IQR) but still captures more relative variability in pollution near interstates than  
 365 monitors (higher CV).

	<b>Road Type</b>	<b>Monitor CV</b>	<b>TROPOMI CV</b>	<b>JSD</b>	<b># of Monitors</b>
a) 50-m Buffer	Interstate	75.07	92.60	0.158	58
	Highway	96.27	91.61	0.095	17
	Non-roadway	118.17	106.16	0.009	428
b) 300-m Buffer	Interstate	77.20	91.014	0.133	91
	Highway	135.76	92.31	0.017	90
	Non-roadway	116.23	108.43	0.008	320

366

367 Table 1. Coefficient of variation and Jensen-Shannon divergence for all seasons combined at  
 368 interstate, highway, and non-roadway monitors 2019-2023 for the 50-m and 300-m roadway  
 369 buffers.

370 The key differences seen within the JSD across the three monitor classifications are also present  
 371 in the percent frequency distributions of NO<sub>2</sub> measured by ground-based monitors and  
 372 TROPOMI (Figure S3), with interstate monitors having the lowest alignment (JSD = 0.158),  
 373 highway monitors having better alignment (JSD = 0.095), and non-roadway monitors having the  
 374 best alignment (JSD = 0.009). The strong alignment between TROPOMI and monitor  
 375 distributions in non-roadway regions is consistent with previous studies (Dressel et al., 2022;  
 376 Kim et al., 2024; Ialongo et al., 2020). This close alignment may be due to the relatively lower  
 377 NO<sub>2</sub> concentrations, which TROPOMI captures more accurately compared to regions with  
 378 higher emissions. These findings further align with previous work showing that TROPOMI tends  
 379 to underestimate NO<sub>2</sub> in high-pollution areas (such as interstates and highways) but slightly  
 380 overestimates in areas of lower pollution, such as rural areas (Dressel et al., 2022; Ialongo et al.,  
 381 2020; Goldberg et al., 2024).

382 Due to the large jump in NO<sub>2</sub> levels seen within Fig. 1 in the 50-300m category, we compare the  
 383 50-meter buffer roadway classifications (Figure S3; Table 1a) with the 300-meter buffer



384 classifications (Figure S4; Table 1b). Notable differences emerge between distributions,  
385 particularly in the highway category, where 73 monitors are added to the highway distribution  
386 (increasing from 17 to 90 monitors; Table 1) due to the larger buffer. The alignment between  
387 monitor data and TROPOMI observations is significantly improved within the 300-meter buffer  
388 near highways. This improvement in alignment is likely due to the decay of NO<sub>2</sub> with increasing  
389 distance from the road (Karner et al., 2010; Kimbrough et al., 2017; Richmond-Bryant et al.,  
390 2017). Consequently, the lower surface NO<sub>2</sub> concentrations observed at 300 meters are better  
391 captured by TROPOMI. This is reflected in Table 2, which shows a substantial reduction in the  
392 JSD for highway monitors, from 0.095 in the 50-meter buffer to 0.017 in the 300-meter buffer  
393 (an 82% increase in alignment at the 300-meter buffer).

394 The differences observed in the highway category with the 300-meter buffer may be present  
395 since the distribution includes 73 more monitors than the 50-meter buffer, capturing lower NO<sub>2</sub>  
396 amounts that are more aligned with TROPOMI's observations. On the other hand, the interstates  
397 category exhibits less noticeable change, with only 33 additional monitors in the 300-meter  
398 buffer distribution (increasing from 58 in the 50-meter buffer, Table 1a; to 91 in the 300-meter  
399 buffer, Table 1b). This suggests that the monitors added in the 300-meter buffer for interstates  
400 measure NO<sub>2</sub> levels similar to those already captured in the 50-meter buffer, resulting in little  
401 change to the overall distribution.

402 These results indicate that TROPOMI follows the trend of NO<sub>2</sub> decreasing with increasing  
403 distance from roadways that ground-based monitors record, and TROPOMI captures surface  
404 concentrations best in winter and at 300+ meters away from the traffic source.

405

### 406 **3.2 Column-Column Daily Alignment**

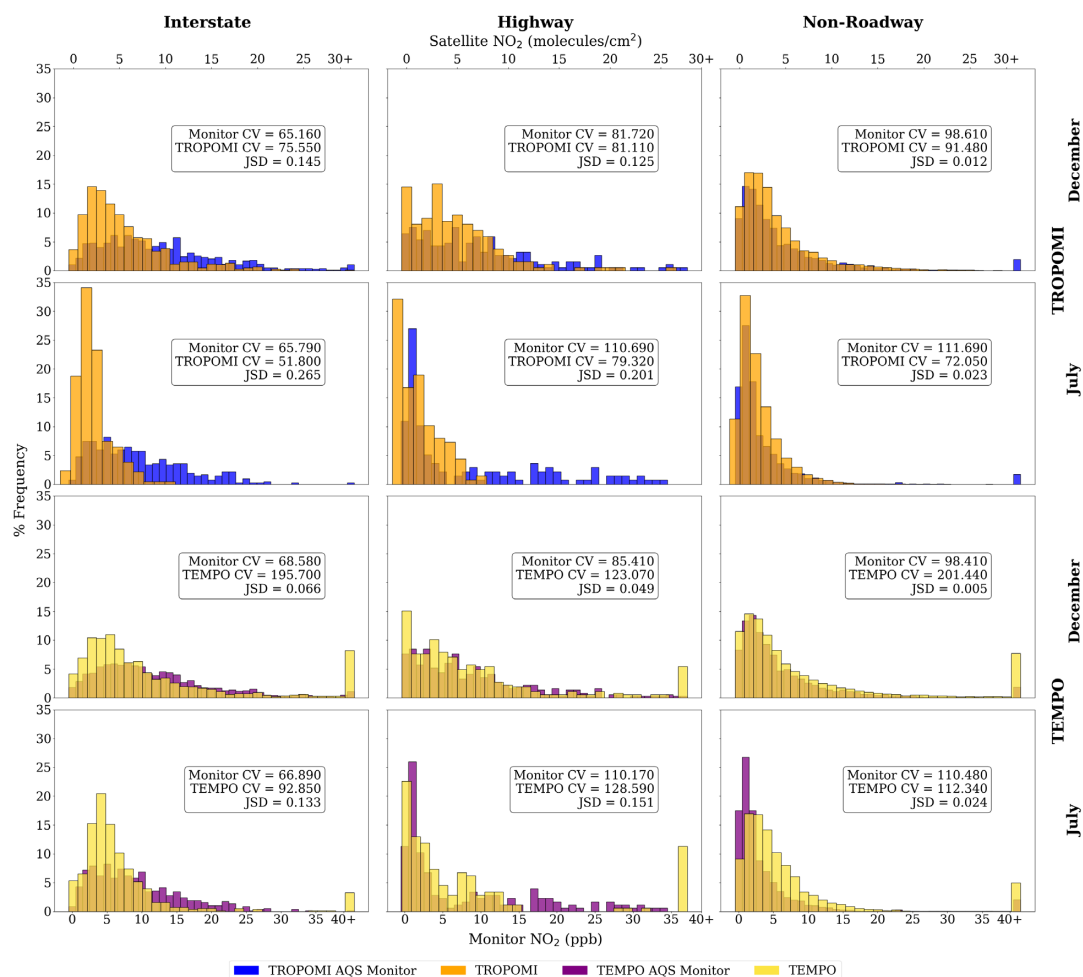
407 Figure 3 shows the distributions of NO<sub>2</sub> as measured by AQS ground-based monitors (filtered to  
408 match valid TROPOMI and TEMPO data), TROPOMI, and TEMPO, separated by road  
409 classifications (interstates, highways, and non-roadways) for December 2023 and July 2024. The  
410 monitor data in each comparison differs due to the data filtering (see Sect. 2.2 and 2.3). The  
411 comparison of frequency distributions reveals how well TEMPO and TROPOMI capture the  
412 wide range of ground-based monitor readings across these classifications and time periods.





413 In December 2023, TEMPO (JSD = 0.007) and TROPOMI (JSD = 0.021) across road  
414 classifications show distinct patterns in their ability to represent NO<sub>2</sub> distributions across road  
415 classifications. Near interstates TEMPO shows a 90<sup>th</sup> percentile at 18.34 x 10<sup>15</sup> molecules/cm<sup>2</sup>  
416 where the TROPOMI 90<sup>th</sup> percentile is 11.27 x 10<sup>15</sup> molecules/cm<sup>2</sup>. TEMPO aligns more closely  
417 with monitor distributions with a JSD of 0.066 compared to the TROPOMI JSD of 0.145 (Figure  
418 3). TEMPO has 21.42% of data points above 11 x 10<sup>15</sup> molecules/cm<sup>2</sup> for interstate values in  
419 December, whereas TROPOMI appears to underestimate the frequency of higher NO<sub>2</sub> levels  
420 more, with a cumulative frequency of 10.53% above that threshold. Near highways, the TEMPO  
421 90<sup>th</sup> percentile is 14.70 x 10<sup>15</sup> molecules/cm<sup>2</sup> compared to TROPOMI with a 90<sup>th</sup> percentile of  
422 10.06 x 10<sup>15</sup> molecules/cm<sup>2</sup>. The JSD for TEMPO is 0.049 and TROPOMI is 0.125 for highway  
423 monitors, indicating that TEMPO has much better alignment on highways (Figure 3). For non-  
424 roadway locations, both instruments show very good alignment (TEMPO JSD = 0.005;  
425 TROPOMI JSD = 0.012; Figure 3) with the monitor data distributions, but with TEMPO again  
426 being slightly better.

427 In July 2024, the patterns show greater divergence across road classifications (TEMPO JSD =  
428 0.027; TROPOMI JSD = 0.049) between the satellite observations and ground-based monitor  
429 data compared to the December 2023 distributions. Near interstates, the TEMPO 90<sup>th</sup> percentile  
430 is 8.46 x 10<sup>15</sup> molecules/cm<sup>2</sup> and the TROPOMI 90<sup>th</sup> percentile is 5.58 x 10<sup>15</sup> molecules/cm<sup>2</sup>,  
431 with TEMPO aligning more closely (JSD of 0.133 compared to TROPOMI JSD of 0.265; Figure  
432 3). TEMPO has 17.01% of data points above 7 x 10<sup>15</sup> molecules/cm<sup>2</sup> for interstate values in July,  
433 whereas TROPOMI appears to underestimate the frequency of higher NO<sub>2</sub> levels more, with a  
434 cumulative frequency of 3.61% above that threshold. Near highways, TEMPO achieves a much  
435 better representation of the higher observed NO<sub>2</sub> with a 90<sup>th</sup> percentile of 9.34 x 10<sup>15</sup>  
436 molecules/cm<sup>2</sup> compared to TROPOMI with a 90<sup>th</sup> percentile of 5.32 x 10<sup>15</sup> molecules/cm<sup>2</sup>. The  
437 JSD for TEMPO is 0.151 and TROPOMI is 0.201 for highway monitors, indicating that TEMPO  
438 has better alignment near highways. For non-roadway locations, both instruments show very  
439 good alignment (TEMPO JSD = 0.024; TROPOMI JSD = 0.023; Figure 3) with the monitor data  
440 distributions, with TEMPO and TROPOMI alignment with ground monitors being more  
441 comparable than in December 2023.



442

443 Figure 3. December 2023 and July 2024 frequency distributions of NO<sub>2</sub> as measured by AQS  
 444 ground-based monitors filtered to the valid TROPOMI (blue) and TEMPO (purple), TROPOMI  
 445 (light orange), and TEMPO (yellow) data for three monitor classifications: Interstate, Highway,  
 446 and Non-roadway. The x-axes indicate the range of NO<sub>2</sub>, with the primary, lower x-axis showing  
 447 monitor NO<sub>2</sub> concentrations in parts per billion (ppb) and the secondary, upper x-axis showing  
 448 TROPOMI NO<sub>2</sub> VCD and TEMPO NO<sub>2</sub> VCD in 10<sup>15</sup> molecules per cm<sup>2</sup>. The boxes show the  
 449 Coefficient of Variation (CV) and Jensen Shannon Divergence (JSD) for each season and  
 450 monitor classification.



451 Throughout both December 2023 and July 2024, TEMPO’s improved alignment with ground-  
452 based monitors compared to TROPOMI may be attributed to several factors. TEMPO operates  
453 from a geostationary orbit, allowing it to take hourly measurements and capture the diurnal  
454 variability of NO<sub>2</sub> concentrations more effectively than TROPOMI, which has a single daily  
455 overpass time. This high temporal resolution enables TEMPO to better match the timing of NO<sub>2</sub>  
456 peaks and fluctuations detected by ground-based monitors, which are also recorded on an hourly  
457 basis. Additionally, TEMPO’s finer spatial resolution, approximately 2 km in the north-south  
458 direction and 4.5 km in the east-west direction, may allow it to capture more localized pollution  
459 sources, such as traffic emissions along highways and interstates. This may be why we see such a  
460 large difference in alignment in the interstate and highway categories between TEMPO and  
461 TROPOMI, and very little difference in alignment in the non-road category. In contrast,  
462 TROPOMI’s 4 km x 4 km (re-gridded) resolution and single overpass time may be less effective  
463 at capturing these localized variations. TEMPO’s finer resolution in one direction and its frequent  
464 observations may enable it to more precisely match the spatial and temporal variability detected  
465 by ground-based monitors. The consistency of slight underestimation for both instruments in  
466 high-pollution areas like highways and interstates suggests challenges in fully capturing elevated  
467 NO<sub>2</sub> levels that occur near traffic sources. Overall, this indicates that while TEMPO generally  
468 provides a closer approximation of NO<sub>2</sub> distributions compared to TROPOMI, both satellite  
469 instruments show limitations, particularly in representing peak concentrations at high-polluting  
470 sites.

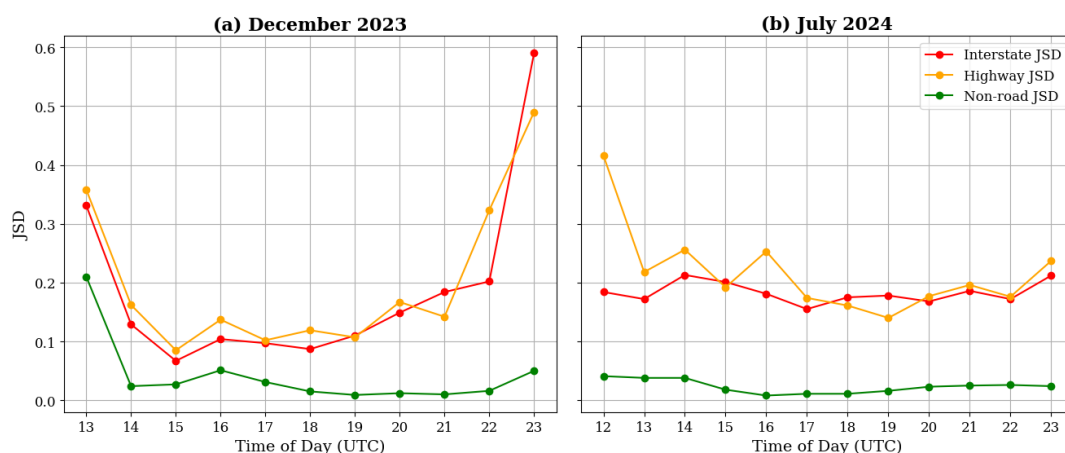
471

### 472 **3.3 Column-Surface Diurnal Alignment**

473 In this section we explore the hourly alignment among monitor observations and TEMPO  
474 observations. Figure 4 presents the hourly JSD for TEMPO NO<sub>2</sub> measurements compared with  
475 ground monitors categorized by interstate (red), highway (orange), and non-roadway (green)  
476 monitors for December 2023 (Figure 4a) and July 2024 (Figure 4b). The results highlight distinct  
477 diurnal patterns across road types and seasons, reflecting the influence of traffic emissions,  
478 atmospheric mixing, and insolation.



479 In December 2023, all monitor categories exhibit similar trends in the early morning, with high  
480 JSD values (highway JSD = 0.358; interstate JSD = 0.331; non-road JSD = 0.210) indicative of  
481 moderate to poor alignment between TEMPO and ground-based monitors. This pattern,  
482 consistent with early morning rush hour emissions and limited atmospheric vertical mixing  
483 (Harkey and Holloway, 2024) as well as a decrease in TEMPO's measurement accuracy due to  
484 high solar zenith angles in the morning according to TEMPO documentation (NASA Langley  
485 Research Center, 2024), suggests that TEMPO may not capture rapid increases in NO<sub>2</sub> during  
486 high traffic and low mixing periods. By mid-morning, JSD has decreased for all road types  
487 (highway JSD = 0.085; interstate JSD = 0.067; non-road JSD = 0.027), indicative of good  
488 alignment, with non-road monitors showing the most significant improvement (87% increase in  
489 alignment). This pattern of better alignment in non-road monitor areas could be attributed to  
490 lower NO<sub>2</sub> levels away from major sources of emissions. As the day progresses in December,  
491 JSD values for highway and interstate monitors increase steadily (with highways fluctuating  
492 more) after 17 UTC (~12 pm LT), with highways increasing in JSD from 0.102 to 0.490 and  
493 interstates increasing from JSD 0.097 to 0.590, indicating worsening alignment in the afternoon  
494 and early evening. This pattern may reflect the re-accumulation of NO<sub>2</sub> due to afternoon traffic  
495 and the collapse of the boundary layer later in the afternoon (Harkey and Holloway, 2024), as  
496 well as the decrease in TEMPO's measurement accuracy in the evening (NASA Langley  
497 Research Center, 2024). Non-road monitors show less change in JSD through the day, suggesting  
498 that TEMPO alignment is more consistent in non-road monitor areas throughout the rest of the  
499 day, only fluctuating in JSD values between 0.009 and 0.05.



500



501 Figure 4. The a) December 2023 and b) July 2024 hourly (UTC) TEMPO NO<sub>2</sub> Jensen-Shannon  
502 Divergences at interstate (red), highway (orange), and non-roadway (green) monitor locations.

503 In July 2024 highway and interstate monitors do not exhibit a clear diurnal pattern, with JSD  
504 values fluctuating between 0.14 and 0.416 for highways and 0.155 and 0.212 for interstates  
505 throughout the day. Consistent, localized traffic emissions and the shorter NO<sub>2</sub> lifetime during  
506 the summer suggest a less variable distribution of NO<sub>2</sub>. Non-road monitors in July show  
507 somewhat worse alignment in the morning (JSD = 0.041), with improved agreement during the  
508 late morning and early afternoon (JSD ranging between 0.008 and 0.025). The non-road JSD  
509 remains fairly constant into the early evening, with alignment decreasing by about 13%,  
510 indicating that sunlight may play a larger role in the alignment in the evening since the sun is at a  
511 higher position in the sky during this time in the summer than in the winter (which increases in  
512 JSD at this time), enhancing TEMPO's measurement accuracy in the early evening in July.

513 Both months exhibit their highest JSDs, and worst alignment, in the early morning or early  
514 evening hours, which coincides with peak traffic times and the most uncertainty in TEMPO  
515 observations caused by the solar zenith angle. The best alignment and lowest JSDs occur  
516 sometime near midday (~10am LT to ~2pm LT).

517 The disparity between highways and interstates in TEMPO, where highways generally have the  
518 highest JSD, differs from the pattern seen with TROPOMI, where interstates tended to  
519 consistently exhibit worse alignment. This suggests that TEMPO's higher spatial and temporal  
520 resolution may capture localized sources more effectively, leading to variations in alignment  
521 based on the distribution and intensity of NO<sub>2</sub> sources.

#### 522 **4 Conclusions**

523 This study evaluates the distributional alignment between satellite-derived NO<sub>2</sub> data from  
524 TROPOMI, TEMPO, and ground-based AQS monitors across the U.S. Our findings highlight  
525 several key points that inform the potential of satellite data for both regulatory and public health  
526 applications, particularly in informing future NO<sub>2</sub> monitor siting strategies.

527 The Jensen-Shannon Divergence (JSD) proved to be an essential tool in this study, offering a  
528 robust and interpretable metric for comparing the alignment and similarity of NO<sub>2</sub> distributions.  
529 Its symmetry and bounded range allowed us to evaluate the degree of similarity between satellite



530 and monitor NO<sub>2</sub> values across different spatial and temporal scales, providing a clear  
531 quantitative framework for assessing the similarity of two different instruments.

532 In this study, we find a pattern of decreasing NO<sub>2</sub> with increasing distance from traffic sources,  
533 which is consistent with the findings of previous studies (Kimbrough et al., 2017; Karner et al.,  
534 2010; Richmond-Bryant et al., 2017). While ground-based monitors and TROPOMI satellite data  
535 may differ with proximity to roadways, particularly within 50-m, their measurements still follow  
536 the same overall trend. This convergence with increasing distance may be due to the reduction of  
537 localized near-road emissions and the broader atmospheric mixing captured more effectively by  
538 satellite observations at greater distances from roads. Using a larger buffer distance from roads  
539 (300 meters instead of 50 meters) improves the alignment between TROPOMI and monitor data,  
540 especially for highway monitor locations (JSD decreases by ~82%). The overall trend reflects the  
541 well-established gradient of declining NO<sub>2</sub> levels with increasing distance from traffic sources,  
542 and TROPOMI's ability to capture this trend, even if the specific values differ from AQS  
543 monitors in the near-road environment. Our findings indicate that TROPOMI tends to slightly  
544 underestimate surface NO<sub>2</sub> concentrations in areas with high traffic, such as interstates and  
545 highways, due to its spatial resolution and full-column measurements, which smooth out  
546 localized, ground-level pollution peaks captured by ground monitors. This is most evident in  
547 interstate monitors, where the JSD reveals the greatest divergence between satellite and monitor  
548 data (JSD = 0.158). These results are consistent with prior studies (Dressel et al., 2022; Kim et  
549 al., 2024; Ialongo et al., 2020), which also found that satellite instruments are less effective at  
550 capturing high NO<sub>2</sub> events near localized sources like traffic. The distributional alignment  
551 improves in non-roadway monitors (JSD = 0.009), where NO<sub>2</sub> levels are lower, and there are  
552 usually fewer localized sources of pollution. The lower pollution levels in these areas allow  
553 TROPOMI to more accurately reflect the conditions captured by ground-based monitors, leading  
554 to lower JSD values, and therefore better alignment. This trend suggests that TROPOMI may be  
555 particularly useful for monitoring air quality in rural or less polluted regions where ground  
556 monitors are sparse or absent.

557 Seasonality plays a critical role in the similarity of satellite and monitor data. Winter consistently  
558 shows the best alignment (JSD = 0.010), with the TROPOMI distribution capturing nearly the  
559 full gradient of NO<sub>2</sub> seen within the ground-based monitor distribution. This likely reflects the



560 longer atmospheric lifetime of NO<sub>2</sub> in winter, which allows for better vertical mixing and less  
561 spatial variability (Harkey et al., 2015; Boersma et al., 2009; Shah et al., 2020). In contrast,  
562 summer shows the worst alignment (JSD = 0.035), which is likely due to the shorter lifetime of  
563 NO<sub>2</sub> and increased photochemical activity during warmer months, causing greater discrepancies  
564 between localized surface measurements and the satellite column. Similar conclusions were  
565 reached by previous studies (Shah et al., 2020; Karagiozidis et al., 2023), indicating that  
566 seasonality is a crucial factor in assessing satellite performance for regulatory purposes. These  
567 seasonal differences underscore the need for considering temporal factors when evaluating the  
568 use of satellite data for monitor siting and NO<sub>2</sub> regulation.

569 The integration of TEMPO data into this study highlights its potential to advance our  
570 understanding of NO<sub>2</sub> distributions, especially when compared to TROPOMI. TEMPO's ability  
571 to provide hourly measurements at a finer spatial resolution offers significant advantages in  
572 capturing diurnal NO<sub>2</sub> patterns and detecting localized pollution events. Our findings from  
573 December 2023 and July 2024 demonstrate that TEMPO better captures the wide range of  
574 surface NO<sub>2</sub> measurements than TROPOMI, especially at higher NO<sub>2</sub> levels. TEMPO's JSDs are  
575 almost always lower than TROPOMI's, with JSDs ranging from 0.005 to 0.151 and TROPOMI's  
576 JSDs ranging from 0.012 to 0.265. This improvement in alignment with ground monitors could  
577 be attributed to TEMPO's better spatial and temporal resolution.

578 We also find that TEMPO is best at capturing ground-level NO<sub>2</sub> amounts around midday (~10am  
579 to ~2pm LT). This could be due to the lower traffic levels and therefore lower pollution levels  
580 during this time period, as well as a lower solar zenith angle, allowing TEMPO to have more  
581 accurate measurements. However, challenges remain in completely capturing high NO<sub>2</sub> levels  
582 during peak traffic times and accurately capturing NO<sub>2</sub> during high solar zenith angles in the  
583 morning and evening across monitor classifications. These results underscore the influence of  
584 spatial resolution, time of day, and measurement frequency on the ability of satellite instruments  
585 to align with ground-based NO<sub>2</sub> measurements. Future research should build upon these insights  
586 by incorporating longer time periods and multiple years of data as more TEMPO data becomes  
587 available to study long-term TEMPO distributions. The enhanced temporal and spatial resolution  
588 of TEMPO, alongside its comparison to other instruments like TROPOMI, provides valuable



589 context for understanding the dynamics of NO<sub>2</sub> pollution, especially how it varies throughout the  
590 day, to improve strategies for air quality monitoring and public health protection.

591 This study offers insights for optimizing nitrogen dioxide monitor siting, enhancing regulatory  
592 planning, and supporting public health interventions. By demonstrating the strengths and  
593 limitations of satellite-derived NO<sub>2</sub> data, we highlight its potential to complement ground-based  
594 monitoring networks.

595

#### 596 **Code and Data Availability**

597 All data used in this study are open to the public. Hourly NO<sub>2</sub> data from AQS were obtained  
598 from [https://aq5.eaa.gov/aqsweb/airdata/download\\_files.html](https://aq5.eaa.gov/aqsweb/airdata/download_files.html). Copernicus Sentinel 5P Level 2  
599 TROPOMI NO<sub>2</sub> data were processed by the ESA, Koninklijk Nederlands Meteorologisch  
600 Instituut (KNMI; <https://doi.org/10.5270/S5P-s4ljg54>), downloaded from the NASA Goddard  
601 Earth Sciences Data and Information Center (GES DISC) in January 2021, and gridded using  
602 WHIPS ([https://sage.nelson.wisc.edu/data-and-models/wisconsin-horizontal-interpolation-  
603 program-for-satellites-whips/](https://sage.nelson.wisc.edu/data-and-models/wisconsin-horizontal-interpolation-program-for-satellites-whips/)). TEMPO Level 3 NO<sub>2</sub> data were downloaded from NASA's  
604 EarthData Search ([https://search.earthdata.nasa.gov/search/granules?p=C2930763263-  
605 LARC\\_CLOUD&pg\[0\]\[v\]=f&tl=1732652660.361!3!!](https://search.earthdata.nasa.gov/search/granules?p=C2930763263-LARC_CLOUD&pg[0][v]=f&tl=1732652660.361!3!!)). Since all of our data is publicly available  
606 and the methods describe our calculations in detail, we did not make our code publicly available.  
607 The Jensen Shannon Divergence was calculated using the *scipy.spatial.distance.jensenshannon*  
608 python package.

609

#### 610 **Author Contribution**

611 SA and TH conceptualized and designed methodology. MH helped with data curation. SA  
612 performed data analysis and visualization and prepared the original draft of the manuscript. All  
613 authors contributed to reviewing and editing the manuscript.

614

#### 615 **Competing Interests**

616 The authors declare that they have no conflict of interest.

617

#### 618 **Acknowledgements**





619 This paper was funded by NASA Grant 80NSSC21K0427 through the Health and Air Quality  
620 Applied Sciences Team (HAQAST). We also thank the EPA for providing the Air Quality System  
621 data, the Earth Sciences Data and Information Center (GES DISC) for TROPOMI L2 data, the  
622 Wisconsin Horizontal Interpolation Program for Satellites (WHIPS) for helping to process and  
623 grid TROPOMI data, and NASA Langley Atmospheric Science Data Center Distributed Active  
624 Archive Center for providing access to the TEMPO data. The authors acknowledge OpenAI 4o  
625 for help with data analysis debugging.

626

627

## 628 **References**

629 Achakulwisut, P., Brauer, M., Hystad, P., and Anenberg, S. C.: Global, national, and urban  
630 burdens of paediatric asthma incidence attributable to ambient NO<sub>2</sub> pollution: estimates from  
631 global datasets, *The Lancet Planetary Health*, 3, e166–e178, [https://doi.org/10.1016/S2542-](https://doi.org/10.1016/S2542-5196(19)30046-4)  
632 [5196\(19\)30046-4](https://doi.org/10.1016/S2542-5196(19)30046-4), 2019.

633 Aerts, S., Haesbroeck, G., and Ruwet, C.: Multivariate coefficients of variation: Comparison and  
634 influence functions, *Journal of Multivariate Analysis*, 142, 183–198,  
635 <https://doi.org/10.1016/j.jmva.2015.08.006>, 2015.

636 Ahmed, Z., Zeeshan, S., Persaud, N., Degroat, W., Abdelhalim, H., and Liang, B. T.:  
637 Investigating genes associated with cardiovascular disease among heart failure patients for  
638 translational research and precision medicine, *Clinical and Translational Dis*, 3, e206,  
639 <https://doi.org/10.1002/ctd2.206>, 2023.

640 Anenberg, S. C., Mohegh, A., Goldberg, D. L., Kerr, G. H., Brauer, M., Burkart, K., Hystad, P.,  
641 Larkin, A., Wozniak, S., and Lamsal, L.: Long-term trends in urban NO<sub>2</sub> concentrations and  
642 associated paediatric asthma incidence: estimates from global datasets, *The Lancet Planetary*  
643 *Health*, 6, e49–e58, [https://doi.org/10.1016/S2542-5196\(21\)00255-2](https://doi.org/10.1016/S2542-5196(21)00255-2), 2022.

644 Wisconsin Horizontal Interpolation Program for Satellites (WHIPS) | Center for Sustainability  
645 and the Global Environment: [https://sage.nelson.wisc.edu/data-and-models/wisconsin-](https://sage.nelson.wisc.edu/data-and-models/wisconsin-horizontal-interpolation-program-for-satellites-whips/)  
646 [horizontal-interpolation-program-for-satellites-whips/](https://sage.nelson.wisc.edu/data-and-models/wisconsin-horizontal-interpolation-program-for-satellites-whips/), last access: 6 December 2024.



- 647 Appel, K. W., Bash, J. O., Fahey, K. M., Foley, K. M., Gilliam, R. C., Hogrefe, C., Hutzell, W.  
648 T., Kang, D., Mathur, R., Murphy, B. N., Napelenok, S. L., Nolte, C. G., Pleim, J. E., Pouliot, G.  
649 A., Pye, H. O. T., Ran, L., Roselle, S. J., Sarwar, G., Schwede, D. B., Sidi, F. I., Spero, T. L., and  
650 Wong, D. C.: The Community Multiscale Air Quality (CMAQ) model versions 5.3 and 5.3.1:  
651 system updates and evaluation, *Geosci. Model Dev.*, 14, 2867–2897,  
652 <https://doi.org/10.5194/gmd-14-2867-2021>, 2021.
- 653 Bai, L., Chen, H., Hatzopoulou, M., Jerrett, M., Kwong, J. C., Burnett, R. T., Van Donkelaar, A.,  
654 Copes, R., Martin, R. V., Van Ryswyk, K., Lu, H., Kopp, A., and Weichenthal, S.: Exposure to  
655 Ambient Ultrafine Particles and Nitrogen Dioxide and Incident Hypertension and Diabetes:,  
656 *Epidemiology*, 29, 323–332, <https://doi.org/10.1097/EDE.0000000000000798>, 2018.
- 657 Bechle, M. J., Millet, D. B., and Marshall, J. D.: Remote sensing of exposure to NO<sub>2</sub>: Satellite  
658 versus ground-based measurement in a large urban area, *Atmospheric Environment*, 69, 345–  
659 353, <https://doi.org/10.1016/j.atmosenv.2012.11.046>, 2013.
- 660 Behera, S. N. and Sharma, M.: Transformation of atmospheric ammonia and acid gases into  
661 components of PM<sub>2.5</sub>: an environmental chamber study, *Environ Sci Pollut Res*, 19, 1187–1197,  
662 <https://doi.org/10.1007/s11356-011-0635-9>, 2012.
- 663 Boersma, K. F., Jacob, D. J., Trainic, M., Rudich, Y., DeSmedt, I., Dirksen, R., and Eskes, H. J.:  
664 Validation of urban NO<sub>2</sub> concentrations and their diurnal and seasonal  
665 variations observed from the SCIAMACHY and OMI sensors using in situ surface  
666 measurements in Israeli cities, *Atmos. Chem. Phys.*, 9, 3867–3879, [https://doi.org/10.5194/acp-](https://doi.org/10.5194/acp-9-3867-2009)  
667 [9-3867-2009](https://doi.org/10.5194/acp-9-3867-2009), 2009.
- 668 Boersma, K. F., Eskes, H. J., Richter, A., De Smedt, I., Lorente, A., Beirle, S., Van Geffen, J. H.  
669 G. M., Zara, M., Peters, E., Van Roozendaal, M., Wagner, T., Maasackers, J. D., Van Der A, R. J.,  
670 Nightingale, J., De Rudder, A., Irie, H., Pinardi, G., Lambert, J.-C., and Compernolle, S. C.:  
671 Improving algorithms and uncertainty estimates for satellite NO<sub>2</sub>  
672 retrievals: results from the quality assurance for the essential climate variables (QA4ECV)  
673 project, *Atmos. Meas. Tech.*, 11, 6651–6678, <https://doi.org/10.5194/amt-11-6651-2018>, 2018.



- 674 Camilleri, S. F., Kerr, G. H., Anenberg, S. C., and Horton, D. E.: All-Cause NO<sub>2</sub> -Attributable  
675 Mortality Burden and Associated Racial and Ethnic Disparities in the United States, *Environ.*  
676 *Sci. Technol. Lett.*, 10, 1159–1164, <https://doi.org/10.1021/acs.estlett.3c00500>, 2023.
- 677 Chance, K., Liu, X., Miller, C. C., González Abad, G., Huang, G., Nowlan, C., Souri, A.,  
678 Suleiman, R., Sun, K., Wang, H., Zhu, L., Zoogman, P., Al-Saadi, J., Antuña-Marrero, J.-C., Carr,  
679 J., Chatfield, R., Chin, M., Cohen, R., Edwards, D., Fishman, J., Flittner, D., Geddes, J., Grutter,  
680 M., Herman, J. R., Jacob, D. J., Janz, S., Joiner, J., Kim, J., Krotkov, N. A., Lefer, B., Martin, R.  
681 V., Mayol-Bracero, O. L., Naeger, A., Newchurch, M., Pfister, G. G., Pickering, K., Pierce, R. B.,  
682 Rivera Cárdenas, C., Saiz-Lopez, A., Simpson, W., Spinei, E., Spurr, R. J. D., Szykman, J. J.,  
683 Torres, O., and Wang, J.: TEMPO Green Paper: Chemistry, physics, and meteorology  
684 experiments with the Tropospheric Emissions: monitoring of pollution instrument, in: *Sensors,*  
685 *Systems, and Next-Generation Satellites XXIII, Sensors, Systems, and Next-Generation*  
686 *Satellites XXIII, Strasbourg, France*, 10, <https://doi.org/10.1117/12.2534883>, 2019.
- 687 Chowdhury, S., Haines, A., Klingmüller, K., Kumar, V., Pozzer, A., Venkataraman, C., Witt, C.,  
688 and Lelieveld, J.: Global and national assessment of the incidence of asthma in children and  
689 adolescents from major sources of ambient NO<sub>2</sub>, *Environ. Res. Lett.*, 16, 035020,  
690 <https://doi.org/10.1088/1748-9326/abe909>, 2021.
- 691 Clim, A., Zota, R. D., and TinicĂ, G.: The Kullback-Leibler Divergence Used in Machine  
692 Learning Algorithms for Health Care Applications and Hypertension Prediction: A Literature  
693 Review, *Procedia Computer Science*, 141, 448–453, <https://doi.org/10.1016/j.procs.2018.10.144>,  
694 2018.
- 695 Cooper, M. J., Martin, R. V., McLinden, C. A., and Brook, J. R.: Inferring ground-level nitrogen  
696 dioxide concentrations at fine spatial resolution applied to the TROPOMI satellite instrument,  
697 *Environ. Res. Lett.*, 15, 104013, <https://doi.org/10.1088/1748-9326/aba3a5>, 2020.
- 698 Dressel, I. M., Demetillo, M. A. G., Judd, L. M., Janz, S. J., Fields, K. P., Sun, K., Fiore, A. M.,  
699 McDonald, B. C., and Pusede, S. E.: Daily Satellite Observations of Nitrogen Dioxide Air  
700 Pollution Inequality in New York City, New York and Newark, New Jersey: Evaluation and  
701 Application, *Environ. Sci. Technol.*, 56, 15298–15311, <https://doi.org/10.1021/acs.est.2c02828>,  
702 2022.



- 703 Duncan, B. N., Yoshida, Y., De Foy, B., Lamsal, L. N., Streets, D. G., Lu, Z., Pickering, K. E.,  
704 and Krotkov, N. A.: The observed response of Ozone Monitoring Instrument (OMI) NO<sub>2</sub>  
705 columns to NO<sub>x</sub> emission controls on power plants in the United States: 2005–2011,  
706 *Atmospheric Environment*, 81, 102–111, <https://doi.org/10.1016/j.atmosenv.2013.08.068>, 2013.
- 707 Duncan, B. N., Prados, A. I., Lamsal, L. N., Liu, Y., Streets, D. G., Gupta, P., Hilsenrath, E.,  
708 Kahn, R. A., Nielsen, J. E., Beyersdorf, A. J., Burton, S. P., Fiore, A. M., Fishman, J., Henze, D.  
709 K., Hostetler, C. A., Krotkov, N. A., Lee, P., Lin, M., Pawson, S., Pfister, G., Pickering, K. E.,  
710 Pierce, R. B., Yoshida, Y., and Ziemba, L. D.: Satellite data of atmospheric pollution for U.S. air  
711 quality applications: Examples of applications, summary of data end-user resources, answers to  
712 FAQs, and common mistakes to avoid, *Atmospheric Environment*, 94, 647–662,  
713 <https://doi.org/10.1016/j.atmosenv.2014.05.061>, 2014.
- 714 Dunlea, E. J., Herndon, S. C., Nelson, D. D., Volkamer, R. M., San Martini, F., Sheehy, P. M.,  
715 Zahniser, M. S., Shorter, J. H., Wormhoudt, J. C., Lamb, B. K., Allwine, E. J., Gaffney, J. S.,  
716 Marley, N. A., Grutter, M., Marquez, C., Blanco, S., Cardenas, B., Retama, A., Ramos Villegas,  
717 C. R., Kolb, C. E., Molina, L. T., and Molina, M. J.: Evaluation of nitrogen dioxide  
718 chemiluminescence monitors in a polluted urban environment, *Atmos. Chem. Phys.*, 7, 2691–  
719 2704, <https://doi.org/10.5194/acp-7-2691-2007>, 2007.
- 720 European Space Agency: TROPOMI Level 2 Nitrogen Dioxide, [https://doi.org/10.5270/S5P-](https://doi.org/10.5270/S5P-9bnp8q8)  
721 [9bnp8q8](https://doi.org/10.5270/S5P-9bnp8q8), 2021.
- 722 Fontijn, Arthur., Sabadell, A. J., and Ronco, R. J.: Homogeneous chemiluminescent measurement  
723 of nitric oxide with ozone. Implications for continuous selective monitoring of gaseous air  
724 pollutants, *Anal. Chem.*, 42, 575–579, <https://doi.org/10.1021/ac60288a034>, 1970.
- 725 Frost, G. J., McKeen, S. A., Trainer, M., Ryerson, T. B., Neuman, J. A., Roberts, J. M., Swanson,  
726 A., Holloway, J. S., Sueper, D. T., Fortin, T., Parrish, D. D., Fehsenfeld, F. C., Flocke, F.,  
727 Peckham, S. E., Grell, G. A., Kowal, D., Cartwright, J., Auerbach, N., and Habermann, T.:  
728 Effects of changing power plant NO<sub>x</sub> emissions on ozone in the eastern United States: Proof of  
729 concept, *J. Geophys. Res.*, 111, 2005JD006354, <https://doi.org/10.1029/2005JD006354>, 2006.



- 730 Gantt, B., Owen, R. C., and Watkins, N.: Characterizing Nitrogen Oxides and Fine Particulate  
731 Matter near Major Highways in the United States Using the National Near-Road Monitoring  
732 Network, *Environ. Sci. Technol.*, 55, 2831–2838, <https://doi.org/10.1021/acs.est.0c05851>, 2021.
- 733 Ge, B., Sun, Y., Liu, Y., Dong, H., Ji, D., Jiang, Q., Li, J., and Wang, Z.: Nitrogen dioxide  
734 measurement by cavity attenuated phase shift spectroscopy (CAPS) and implications in ozone  
735 production efficiency and nitrate formation in Beijing, China, *JGR Atmospheres*, 118, 9499–  
736 9509, <https://doi.org/10.1002/jgrd.50757>, 2013.
- 737 Goldberg, D. L., Anenberg, S. C., Kerr, G. H., Mohegh, A., Lu, Z., and Streets, D. G.:  
738 TROPOMI NO<sub>2</sub> in the United States: A Detailed Look at the Annual Averages, Weekly Cycles,  
739 Effects of Temperature, and Correlation With Surface NO<sub>2</sub> Concentrations, *Earth’s Future*, 9,  
740 e2020EF001665, <https://doi.org/10.1029/2020EF001665>, 2021.
- 741 Goldberg, D. L., Tao, M., Kerr, G. H., Ma, S., Tong, D. Q., Fiore, A. M., Dickens, A. F.,  
742 Adelman, Z. E., and Anenberg, S. C.: Evaluating the spatial patterns of U.S. urban NO<sub>x</sub>  
743 emissions using TROPOMI NO<sub>2</sub>, *Remote Sensing of Environment*, 300, 113917,  
744 <https://doi.org/10.1016/j.rse.2023.113917>, 2024.
- 745 Griffin, D., Zhao, X., McLinden, C. A., Boersma, F., Bourassa, A., Dammers, E., Degenstein, D.,  
746 Eskes, H., Fehr, L., Fioletov, V., Hayden, K., Kharol, S. K., Li, S., Makar, P., Martin, R. V.,  
747 Mihele, C., Mittermeier, R. L., Krotkov, N., Sneep, M., Lamsal, L. N., Linden, M. T., Geffen, J.  
748 V., Veefkind, P., and Wolde, M.: High-Resolution Mapping of Nitrogen Dioxide With  
749 TROPOMI: First Results and Validation Over the Canadian Oil Sands, *Geophysical Research*  
750 *Letters*, 46, 1049–1060, <https://doi.org/10.1029/2018GL081095>, 2019.
- 751 Grulke, N. E. and Heath, R. L.: Ozone effects on plants in natural ecosystems, *Plant Biol J*, 22,  
752 12–37, <https://doi.org/10.1111/plb.12971>, 2020.
- 753 Hales, S., Atkinson, J., Metcalfe, J., Kuschel, G., and Woodward, A.: Long term exposure to air  
754 pollution, mortality and morbidity in New Zealand: Cohort study, *Science of The Total*  
755 *Environment*, 801, 149660, <https://doi.org/10.1016/j.scitotenv.2021.149660>, 2021.



- 756 Harkey, M. and Holloway, T.: Simulated Surface-Column NO<sub>2</sub> Connections for Satellite  
757 Applications, JGR Atmospheres, 129, e2024JD041912, <https://doi.org/10.1029/2024JD041912>,  
758 2024.
- 759 Harkey, M., Holloway, T., Oberman, J., and Scotty, E.: An evaluation of CMAQ NO<sub>2</sub> using  
760 observed chemistry-meteorology correlations, JGR Atmospheres, 120,  
761 <https://doi.org/10.1002/2015JD023316>, 2015.
- 762 Holloway, T., Miller, D., Anenberg, S., Diao, M., Duncan, B., Fiore, A. M., Henze, D. K., Hess,  
763 J., Kinney, P. L., Liu, Y., Neu, J. L., O'Neill, S. M., Odman, M. T., Pierce, R. B., Russell, A. G.,  
764 Tong, D., West, J. J., and Zondlo, M. A.: Satellite Monitoring for Air Quality and Health, Annu.  
765 Rev. Biomed. Data Sci., 4, 417–447, <https://doi.org/10.1146/annurev-biodatasci-110920-093120>,  
766 2021.
- 767 Huangfu, P. and Atkinson, R.: Long-term exposure to NO<sub>2</sub> and O<sub>3</sub> and all-cause and respiratory  
768 mortality: A systematic review and meta-analysis, Environment International, 144, 105998,  
769 <https://doi.org/10.1016/j.envint.2020.105998>, 2020.
- 770 Ialongo, I., Virta, H., Eskes, H., Hovila, J., and Douros, J.: Comparison of TROPOMI/Sentinel-5  
771 Precursor NO<sub>2</sub> observations with ground-based measurements in  
772 Helsinki, Atmos. Meas. Tech., 13, 205–218, <https://doi.org/10.5194/amt-13-205-2020>, 2020.
- 773 Jia, M., Wang, Z., Wang, C., Mao, D., and Zhang, Y.: A New Vegetation Index to Detect  
774 Periodically Submerged Mangrove Forest Using Single-Tide Sentinel-2 Imagery, Remote  
775 Sensing, 11, 2043, <https://doi.org/10.3390/rs11172043>, 2019.
- 776 Jones, D. C., Danaher, P., Kim, Y., Beechem, J. M., Gottardo, R., and Newell, E. W.: An  
777 information theoretic approach to detecting spatially varying genes, Cell Reports Methods, 3,  
778 100507, <https://doi.org/10.1016/j.crmeth.2023.100507>, 2023.
- 779 Karagkiozidis, D., Koukouli, M.-E., Bais, A., Balis, D., and Tzoumaka, P.: Assessment of the  
780 NO<sub>2</sub> Spatio-Temporal Variability over Thessaloniki, Greece, Using MAX-DOAS Measurements  
781 and Comparison with S5P/TROPOMI Observations, Applied Sciences, 13, 2641,  
782 <https://doi.org/10.3390/app13042641>, 2023.



- 783 Karner, A. A., Eisinger, D. S., and Niemeier, D. A.: Near-Roadway Air Quality: Synthesizing the  
784 Findings from Real-World Data, *Environ. Sci. Technol.*, 44, 5334–5344,  
785 <https://doi.org/10.1021/es100008x>, 2010.
- 786 Keabian, P. L., Herndon, S. C., and Freedman, A.: Detection of Nitrogen Dioxide by Cavity  
787 Attenuated Phase Shift Spectroscopy, *Anal. Chem.*, 77, 724–728,  
788 <https://doi.org/10.1021/ac048715y>, 2005.
- 789 Kibirige, G. W., Huang, C. C., Liu, C. L., and Chen, M. C.: Influence of land-sea breeze on  
790 PM<sub>2.5</sub> prediction in central and southern Taiwan using composite neural network, *Sci*  
791 *Rep*, 13, 3827, <https://doi.org/10.1038/s41598-023-29845-w>, 2023.
- 792 Kim, E. J., Holloway, T., Kokandakar, A., Harkey, M., Elkins, S., Goldberg, D. L., and Heck, C.:  
793 A Comparison of Regression Methods for Inferring Near-Surface NO<sub>2</sub> With Satellite Data, *JGR*  
794 *Atmospheres*, 129, e2024JD040906, <https://doi.org/10.1029/2024JD040906>, 2024.
- 795 Kim, H. C., Kim, S., Lee, S.-H., Kim, B.-U., and Lee, P.: Fine-Scale Columnar and Surface NO<sub>x</sub>  
796 Concentrations over South Korea: Comparison of Surface Monitors, TROPOMI, CMAQ and  
797 CAPSS Inventory, *Atmosphere*, 11, 101, <https://doi.org/10.3390/atmos11010101>, 2020.
- 798 Kim, M., Brunner, D., and Kuhlmann, G.: Importance of satellite observations for high-  
799 resolution mapping of near-surface NO<sub>2</sub> by machine learning, *Remote Sensing of Environment*,  
800 264, 112573, <https://doi.org/10.1016/j.rse.2021.112573>, 2021.
- 801 Kimbrough, S., Chris Owen, R., Snyder, M., and Richmond-Bryant, J.: NO to NO<sub>2</sub> conversion  
802 rate analysis and implications for dispersion model chemistry methods using Las Vegas, Nevada  
803 near-road field measurements, *Atmospheric Environment*, 165, 23–34,  
804 <https://doi.org/10.1016/j.atmosenv.2017.06.027>, 2017.
- 805 Knox, J. B. and Lange, R.: Surface Air Pollutant Concentration Frequency Distributions:  
806 Implications for Urban Modeling, *Journal of the Air Pollution Control Association*, 24, 48–53,  
807 <https://doi.org/10.1080/00022470.1974.10469893>, 1974.
- 808 Lamsal, L. N., Krotkov, N. A., Celarier, E. A., Swartz, W. H., Pickering, K. E., Bucsela, E. J.,  
809 Gleason, J. F., Martin, R. V., Philip, S., Irie, H., Cede, A., Herman, J., Weinheimer, A., Szykman,  
810 J. J., and Knepp, T. N.: Evaluation of OMI operational standard NO<sub>2</sub> retrieval, *Atmospheric Chemistry and Physics*, 12, 1111–1124, <https://doi.org/10.5194/acp-12-1111-2012>, 2012.



- 811 column retrievals using in situ and surface-based NO<sub>2</sub> observations,  
812 Atmos. Chem. Phys., 14, 11587–11609, <https://doi.org/10.5194/acp-14-11587-2014>, 2014.
- 813 Lamsal, L. N., Duncan, B. N., Yoshida, Y., Krotkov, N. A., Pickering, K. E., Streets, D. G., and  
814 Lu, Z.: U.S. NO<sub>2</sub> trends (2005–2013): EPA Air Quality System (AQS) data versus improved  
815 observations from the Ozone Monitoring Instrument (OMI), Atmospheric Environment, 110,  
816 130–143, <https://doi.org/10.1016/j.atmosenv.2015.03.055>, 2015.
- 817 Lange, K., Richter, A., and Burrows, J. P.: Variability of nitrogen oxide emission fluxes and  
818 lifetimes estimated from Sentinel-5P TROPOMI observations, Atmos. Chem. Phys., 22, 2745–  
819 2767, <https://doi.org/10.5194/acp-22-2745-2022>, 2022.
- 820 Lee, H. J. and Koutrakis, P.: Daily Ambient NO<sub>2</sub> Concentration Predictions Using Satellite  
821 Ozone Monitoring Instrument NO<sub>2</sub> Data and Land Use Regression, Environ. Sci. Technol.,  
822 140204134232009, <https://doi.org/10.1021/es404845f>, 2014.
- 823 Lee, H. J., Liu, Y., and Chatfield, R. B.: Neighborhood-scale ambient NO<sub>2</sub> concentrations using  
824 TROPOMI NO<sub>2</sub> data: Applications for spatially comprehensive exposure assessment, Science of  
825 The Total Environment, 857, 159342, <https://doi.org/10.1016/j.scitotenv.2022.159342>, 2023.
- 826 Lee, M., Heikes, B. G., Jacob, D. J., Sachse, G., and Anderson, B.: Hydrogen peroxide, organic  
827 hydroperoxide, and formaldehyde as primary pollutants from biomass burning, J. Geophys. Res.,  
828 102, 1301–1309, <https://doi.org/10.1029/96JD01709>, 1997.
- 829 Levelt, P. F., Van Den Oord, G. H. J., Dobber, M. R., Malkki, A., Huib Visser, Johan De Vries,  
830 Stammes, P., Lundell, J. O. V., and Saari, H.: The ozone monitoring instrument, IEEE Trans.  
831 Geosci. Remote Sensing, 44, 1093–1101, <https://doi.org/10.1109/TGRS.2006.872333>, 2006.
- 832 Levinson, R. and Akbari, H.: Potential benefits of cool roofs on commercial buildings:  
833 conserving energy, saving money, and reducing emission of greenhouse gases and air pollutants,  
834 Energy Efficiency, 3, 53–109, <https://doi.org/10.1007/s12053-008-9038-2>, 2010.
- 835 Li, J., Wang, Y., Zhang, R., Smeltzer, C., Weinheimer, A., Herman, J., Boersma, K. F., Celarier,  
836 E. A., Long, R. W., Szykman, J. J., Delgado, R., Thompson, A. M., Knepp, T. N., Lamsal, L. N.,  
837 Janz, S. J., Kowalewski, M. G., Liu, X., and Nowlan, C. R.: Comprehensive evaluations of  
838 diurnal NO<sub>2</sub> measurements during DISCOVER-AQ 2011: effects of





- 839 resolution-dependent representation of NO<sub>x</sub> emissions, *Atmos. Chem. Phys.*, 21, 11133–11160, <https://doi.org/10.5194/acp-21-11133-2021>,  
840 2021.  
841
- 842 Liu, X., Yi, G., Zhou, X., Zhang, T., Lan, Y., Yu, D., Wen, B., and Hu, J.: Atmospheric NO<sub>2</sub>  
843 Distribution Characteristics and Influencing Factors in Yangtze River Economic Belt: Analysis of  
844 the NO<sub>2</sub> Product of TROPOMI/Sentinel-5P, *Atmosphere*, 12, 1142,  
845 <https://doi.org/10.3390/atmos12091142>, 2021.
- 846 Melville, P., Yang, S.M., Saar-Tsechansky, M., Mooney, R.J.: Active Learning for Probability  
847 Estimation using Jensen-Shannon Divergence, in: Proceedings of the 16th European Conference  
848 on Machine Learning, 268–279, 2005.
- 849 Menéndez, M. L., Pardo, J. A., Pardo, L., and Pardo, M. C.: The Jensen-Shannon divergence,  
850 *Journal of the Franklin Institute*, 334, 307–318, [https://doi.org/10.1016/S0016-0032\(96\)00063-4](https://doi.org/10.1016/S0016-0032(96)00063-4),  
851 1997.
- 852 Meng, X., Liu, C., Chen, R., Sera, F., Vicedo-Cabrera, A. M., Milojevic, A., Guo, Y., Tong, S.,  
853 Coelho, M. D. S. Z. S., Saldiva, P. H. N., Lavigne, E., Correa, P. M., Ortega, N. V., Osorio, S.,  
854 Garcia, Kysely, J., Urban, A., Orru, H., Maasikmets, M., Jaakkola, J. J. K., Rytty, N., Huber, V.,  
855 Schneider, A., Katsouyanni, K., Analitis, A., Hashizume, M., Honda, Y., Ng, C. F. S., Nunes, B.,  
856 Teixeira, J. P., Holobaca, I. H., Fratanni, S., Kim, H., Tobias, A., Íñiguez, C., Forsberg, B.,  
857 Åström, C., Ragettli, M. S., Guo, Y.-L. L., Pan, S.-C., Li, S., Bell, M. L., Zanobetti, A., Schwartz,  
858 J., Wu, T., Gasparrini, A., and Kan, H.: Short term associations of ambient nitrogen dioxide with  
859 daily total, cardiovascular, and respiratory mortality: multilocation analysis in 398 cities, *BMJ*,  
860 n534, <https://doi.org/10.1136/bmj.n534>, 2021.
- 861 Mills, I. C., Atkinson, R. W., Kang, S., Walton, H., and Anderson, H. R.: Quantitative systematic  
862 review of the associations between short-term exposure to nitrogen dioxide and mortality and  
863 hospital admissions, *BMJ Open*, 5, e006946, <https://doi.org/10.1136/bmjopen-2014-006946>,  
864 2015.
- 865 Mölter, A., Agius, R., De Vocht, F., Lindley, S., Gerrard, W., Custovic, A., and Simpson, A.:  
866 Effects of long-term exposure to PM<sub>10</sub> and NO<sub>2</sub> on asthma and wheeze in a prospective birth



- 867 cohort, *J Epidemiol Community Health*, 68, 21–28, <https://doi.org/10.1136/jech-2013-202681>,  
868 2014.
- 869 Mondal, A., Sharma, S. K., Mandal, T. K., Girach, I., and Ojha, N.: Frequency distribution of  
870 pollutant concentrations over Indian megacities impacted by the COVID-19 lockdown, *Environ*  
871 *Sci Pollut Res*, 29, 85676–85687, <https://doi.org/10.1007/s11356-021-16874-z>, 2022.
- 872 Naeger, A. R., Newchurch, M. J., Moore, T., Chance, K., Liu, X., Alexander, S., Murphy, K., and  
873 Wang, B.: Revolutionary Air-Pollution Applications from Future Tropospheric Emissions:  
874 Monitoring of Pollution (TEMPO) Observations, *Bulletin of the American Meteorological*  
875 *Society*, 102, E1735–E1741, <https://doi.org/10.1175/BAMS-D-21-0050.1>, 2021.
- 876 Tropospheric Emissions: Monitoring of Pollution (EVI-1) | NASA’s Earth Observing System:  
877 <https://eosps.nasa.gov/missions/tropospheric-emissions-monitoring-pollution-evi-1>, last access:  
878 26 November 2024.
- 879 NASA Langley Research Center: TEMPO Level 2/3 trace gas and cloud data user guide, 2024.
- 880 Novotny, E. V., Bechle, M. J., Millet, D. B., and Marshall, J. D.: National Satellite-Based Land-  
881 Use Regression: NO<sub>2</sub> in the United States, *Environ. Sci. Technol.*, 45, 4407–4414,  
882 <https://doi.org/10.1021/es103578x>, 2011.
- 883 Orellano, P., Reynoso, J., Quaranta, N., Bardach, A., and Ciapponi, A.: Short-term exposure to  
884 particulate matter (PM<sub>10</sub> and PM<sub>2.5</sub>), nitrogen dioxide (NO<sub>2</sub>), and ozone (O<sub>3</sub>) and all-cause and  
885 cause-specific mortality: Systematic review and meta-analysis, *Environment International*, 142,  
886 105876, <https://doi.org/10.1016/j.envint.2020.105876>, 2020.
- 887 Penn, E. and Holloway, T.: Evaluating current satellite capability to observe diurnal change in  
888 nitrogen oxides in preparation for geostationary satellite missions, *Environ. Res. Lett.*, 15,  
889 034038, <https://doi.org/10.1088/1748-9326/ab6b36>, 2020.
- 890 Pollack, R.: *Studies of Pollutant Concentration Frequency Distributions*, 1975.
- 891 Qin, M., Yu, H., Hu, Y., Russell, A. G., Odman, M. T., Doty, K., Pour-Biazar, A., McNider, R. T.,  
892 and Knipping, E.: Improving ozone simulations in the Great Lakes Region: The role of  
893 emissions, chemistry, and dry deposition, *Atmospheric Environment*, 202, 167–179,  
894 <https://doi.org/10.1016/j.atmosenv.2019.01.025>, 2019.



- 895 Richmond-Bryant, J., Chris Owen, R., Graham, S., Snyder, M., McDow, S., Oakes, M., and  
896 Kimbrough, S.: Estimation of on-road NO<sub>2</sub> concentrations, NO<sub>2</sub>/NO<sub>x</sub> ratios, and related  
897 roadway gradients from near-road monitoring data, *Air Qual Atmos Health*, 10, 611–625,  
898 <https://doi.org/10.1007/s11869-016-0455-7>, 2017.
- 899 Richter, A., Burrows, J. P., Nüß, H., Granier, C., and Niemeier, U.: Increase in tropospheric  
900 nitrogen dioxide over China observed from space, *Nature*, 437, 129–132,  
901 <https://doi.org/10.1038/nature04092>, 2005.
- 902 Sangkham, S., Phairuang, W., Sherchan, S. P., Pansakun, N., Munkong, N., Sarndhong, K.,  
903 Islam, Md. A., and Sakunkoo, P.: An update on adverse health effects from exposure to PM<sub>2.5</sub>,  
904 *Environmental Advances*, 18, 100603, <https://doi.org/10.1016/j.envadv.2024.100603>, 2024.
- 905 Saurette, D. D., Heck, R. J., Gillespie, A. W., Berg, A. A., and Biswas, A.: Divergence metrics for  
906 determining optimal training sample size in digital soil mapping, *Geoderma*, 436, 116553,  
907 <https://doi.org/10.1016/j.geoderma.2023.116553>, 2023.
- 908 Shah, V., Jacob, D. J., Li, K., Silvern, R. F., Zhai, S., Liu, M., Lin, J., and Zhang, Q.: Effect of  
909 changing NO<sub>x</sub> lifetime on the seasonality and long-  
910 term trends of satellite-observed tropospheric NO<sub>2</sub> columns over China,  
911 *Atmos. Chem. Phys.*, 20, 1483–1495, <https://doi.org/10.5194/acp-20-1483-2020>, 2020.
- 912 Sharma, S., Chandra, M., and Kota, S. H.: Health Effects Associated with PM<sub>2.5</sub>: a Systematic  
913 Review, *Curr Pollution Rep*, 6, 345–367, <https://doi.org/10.1007/s40726-020-00155-3>, 2020.
- 914 Shetty, S., Schneider, P., Stebel, K., David Hamer, P., Kylling, A., and Koren Berntsen, T.:  
915 Estimating surface NO<sub>2</sub> concentrations over Europe using Sentinel-5P TROPOMI observations  
916 and Machine Learning, *Remote Sensing of Environment*, 312, 114321,  
917 <https://doi.org/10.1016/j.rse.2024.114321>, 2024.
- 918 Sillman, S.: The relation between ozone, NO<sub>x</sub> and hydrocarbons in urban and polluted rural  
919 environments, *Atmospheric Environment*, 33, 1821–1845, [https://doi.org/10.1016/S1352-  
920 2310\(98\)00345-8](https://doi.org/10.1016/S1352-2310(98)00345-8), 1999.
- 921 Steinbacher, M., Zellweger, C., Schwarzenbach, B., Bugmann, S., Buchmann, B., Ordóñez, C.,  
922 Prevot, A. S. H., and Hueglin, C.: Nitrogen oxide measurements at rural sites in Switzerland:



- 923 Bias of conventional measurement techniques, *J. Geophys. Res.*, 112, 2006JD007971,  
924 <https://doi.org/10.1029/2006JD007971>, 2007.
- 925 Suleiman, R.: TEMPO gridded NO<sub>2</sub> tropospheric and stratospheric columns V03  
926 (PROVISIONAL), [https://doi.org/10.5067/IS-40E/TEMPO/NO2\\_L3.003](https://doi.org/10.5067/IS-40E/TEMPO/NO2_L3.003), 2024.
- 927 Thangavel, P., Park, D., and Lee, Y.-C.: Recent Insights into Particulate Matter (PM<sub>2.5</sub>)-  
928 Mediated Toxicity in Humans: An Overview, *IJERPH*, 19, 7511,  
929 <https://doi.org/10.3390/ijerph19127511>, 2022.
- 930 Thiagarajan, P. and Ghosh, S.: Jensen–Shannon divergence based novel loss functions for  
931 Bayesian neural networks, *Neurocomputing*, 618, 129115,  
932 <https://doi.org/10.1016/j.neucom.2024.129115>, 2024.
- 933 Toledo, A. S. O., Silini, R., Carpi, L. C., and Masoller, C.: Outlier mining in high-dimensional  
934 data using the Jensen–Shannon divergence and graph structure analysis, *J. Phys. Complex.*, 3,  
935 045011, <https://doi.org/10.1088/2632-072X/aca94a>, 2022.
- 936 Tsigalou, C., Panopoulou, M., Papadopoulos, C., Karvelas, A., Tsairidis, D., and  
937 Anagnostopoulos, K.: Estimation of low-density lipoprotein cholesterol by machine learning  
938 methods, *Clinica Chimica Acta*, 517, 108–116, <https://doi.org/10.1016/j.cca.2021.02.020>, 2021.
- 939 Urbanowicz, T., Skotak, K., Filipiak, K. J., Ołasińska-Wiśniewska, A., Szczepański, K., Wyrwa,  
940 M., Sikora, J., Tykarski, A., and Jemielity, M.: Long-Term Exposure of Nitrogen Oxides Air  
941 Pollution (NO<sub>2</sub>) Impact for Coronary Artery Lesion Progression—Pilot Study, *JPM*, 13, 1376,  
942 <https://doi.org/10.3390/jpm13091376>, 2023.
- 943 AirNow API Documentation: <https://docs.airnowapi.org/>, last access: 26 November 2024.
- 944 Download Files | AirData | US EPA: [https://aq5.epa.gov/aq5web/airdata/download\\_files.html](https://aq5.epa.gov/aq5web/airdata/download_files.html), last  
945 access: 6 December 2024.
- 946 Van Der A, R. J., Eskes, H. J., Boersma, K. F., Van Noije, T. P. C., Van Roozendaal, M., De  
947 Smedt, I., Peters, D. H. M. U., and Meijer, E. W.: Trends, seasonal variability and dominant NO<sub>x</sub>  
948 source derived from a ten year record of NO<sub>2</sub> measured from space, *J. Geophys. Res.*, 113,  
949 2007JD009021, <https://doi.org/10.1029/2007JD009021>, 2008.



- 950 Van Geffen, J., Boersma, K. F., Eskes, H., Sneep, M., Ter Linden, M., Zara, M., and Veefkind, J.  
951 P.: S5P TROPOMI NO<sub>2</sub> slant column retrieval: method, stability,  
952 uncertainties and comparisons with OMI, *Atmos. Meas. Tech.*, 13, 1315–1335,  
953 <https://doi.org/10.5194/amt-13-1315-2020>, 2020.
- 954 Veefkind, J. P., Aben, I., McMullan, K., Förster, H., De Vries, J., Otter, G., Claas, J., Eskes, H. J.,  
955 De Haan, J. F., Kleipool, Q., Van Weele, M., Hasekamp, O., Hoogeveen, R., Landgraf, J., Snel,  
956 R., Tol, P., Ingmann, P., Voors, R., Kruizinga, B., Vink, R., Visser, H., and Levelt, P. F.:  
957 TROPOMI on the ESA Sentinel-5 Precursor: A GMES mission for global observations of the  
958 atmospheric composition for climate, air quality and ozone layer applications, *Remote Sensing*  
959 *of Environment*, 120, 70–83, <https://doi.org/10.1016/j.rse.2011.09.027>, 2012.
- 960 Venkatram, A.: Applications of Pollutant Frequency Distributions, *Journal of the Air Pollution*  
961 *Control Association*, 29, 251–253, <https://doi.org/10.1080/00022470.1979.10470788>, 1979.
- 962 Virta, H., Ialongo, I., Szeląg, M., and Eskes, H.: Estimating surface-level nitrogen dioxide  
963 concentrations from Sentinel-5P/TROPOMI observations in Finland, *Atmospheric Environment*,  
964 312, 119989, <https://doi.org/10.1016/j.atmosenv.2023.119989>, 2023.
- 965 Wang, F. and Zhang, Z.: Correlation Structure and Co-Movement of Hunan Province’s Air  
966 Pollution: Evidence from the Multiscale Temporal Networks, *Atmosphere*, 14, 55,  
967 <https://doi.org/10.3390/atmos14010055>, 2022.
- 968 Wang, Y., Bechle, M. J., Kim, S.-Y., Adams, P. J., Pandis, S. N., Pope, C. A., Robinson, A. L.,  
969 Sheppard, L., Szpiro, A. A., and Marshall, J. D.: Spatial decomposition analysis of NO<sub>2</sub> and  
970 PM<sub>2.5</sub> air pollution in the United States, *Atmospheric Environment*, 241, 117470,  
971 <https://doi.org/10.1016/j.atmosenv.2020.117470>, 2020.
- 972 Xia, X., Meng, X., Liu, C., Guo, Y., Li, X., Niu, Y., Lam, K. B. H., Wright, N., Kartsonaki, C.,  
973 Chen, Y., Yang, L., Du, H., Yu, C., Sun, D., Lv, J., Chen, J., Yang, X., Gao, R., Wu, S., Kan, H.,  
974 Chan, K. H., Li, L., Chen, Z., Chen, J., Chen, Z., Clarke, R., Collins, R., Li, L., Lv, J., Peto, R.,  
975 Walters, R., EdrisMohamed, A., Pozarickij, A., Iona, A., Wang, B., Clarke, C., Kartsonaki, C.,  
976 Schmidt, D., Avery, D., Bennett, D., Fry, H., Du, H., Lam, H., Turnbull, I., Millwood, I., Liu, J.,  
977 Clarke, J., Chan, K. H., Kolhe, K., Lin, K., Wang, L., Yang, L., Kakkoura, M., Rahmati, M.,  
978 Barnard, M., Mazidi, M., Wright, N., Yao, P., Ryder, P., Im, P. K., Harish, P., Nie, Q., Stevens, R.,



- 979 Clarke, R., Walters, R., Boxall, R., Morris, S., Gilbert, S., Yang, X., Chen, Y., Chen, Z., Han, X.,  
980 Hou, C., Xia, Q., Liu, C., Lv, J., Pei, P., Sun, D., Yu, C., Pan, L., Pang, Z., Gao, R., Li, S., Duan,  
981 H., Wang, S., Liu, Y., Du, R., Zang, Y., Cheng, L., Tian, X., Zhang, H., Zhai, Y., Ning, F., Sun,  
982 X., Li, F., Lv, S., Wang, J., Hou, W., Sun, W., et al.: Associations of long-term nitrogen dioxide  
983 exposure with a wide spectrum of diseases: a prospective cohort study of 0·5 million Chinese  
984 adults, *The Lancet Public Health*, 9, e1047–e1058, [https://doi.org/10.1016/S2468-](https://doi.org/10.1016/S2468-2667(24)00264-0)  
985 [2667\(24\)00264-0](https://doi.org/10.1016/S2468-2667(24)00264-0), 2024.
- 986 Xu, A. and Xiang, C.: Assessment of the Emission Characteristics of Major States in the United  
987 States using Satellite Observations of CO<sub>2</sub>, CO, and NO<sub>2</sub>, *Atmosphere*, 15, 11,  
988 <https://doi.org/10.3390/atmos15010011>, 2023.
- 989 Yan, J., Li, P., Gao, R., Li, Y., and Chen, L.: Identifying Critical States of Complex Diseases by  
990 Single-Sample Jensen-Shannon Divergence, *Front. Oncol.*, 11, 684781,  
991 <https://doi.org/10.3389/fonc.2021.684781>, 2021.
- 992 Yu, Z. and Li, X.: The Temporal–Spatial Characteristics of Column NO<sub>2</sub> Concentration and  
993 Influence Factors in Xinjiang of Northwestern Arid Region in China, *Atmosphere*, 13, 1533,  
994 <https://doi.org/10.3390/atmos13101533>, 2022.
- 995 Zhang, R., Wang, Y., Smeltzer, C., Qu, H., Koshak, W., and Boersma, K. F.: Reconciling the  
996 differences between OMI-based and EPA AQS in situ NO<sub>2</sub> trends,  
997 <https://doi.org/10.5194/amt-2017-410>, 25 January 2018.
- 998 Zhao, D., Yan, W., You, M., Zhang, J., Arun, P. V., Jiao, C., Wang, Q., and Zhou, H.:  
999 Hyperspectral Anomaly Detection Based on Empirical Mode Decomposition and Local  
1000 Weighted Contrast, *IEEE Sensors J.*, 24, 33847–33861,  
1001 <https://doi.org/10.1109/JSEN.2024.3455258>, 2024.
- 1002 Zoogman, P., Liu, X., Suleiman, R. M., Pennington, W. F., Flittner, D. E., Al-Saadi, J. A., Hilton,  
1003 B. B., Nicks, D. K., Newchurch, M. J., Carr, J. L., Janz, S. J., Andraschko, M. R., Arola, A.,  
1004 Baker, B. D., Canova, B. P., Chan Miller, C., Cohen, R. C., Davis, J. E., Dussault, M. E.,  
1005 Edwards, D. P., Fishman, J., Ghulam, A., González Abad, G., Grutter, M., Herman, J. R., Houck,  
1006 J., Jacob, D. J., Joiner, J., Kerridge, B. J., Kim, J., Krotkov, N. A., Lamsal, L., Li, C., Lindfors,  
1007 A., Martin, R. V., McElroy, C. T., McLinden, C., Natraj, V., Neil, D. O., Nowlan, C. R.,



1008 O'Sullivan, E. J., Palmer, P. I., Pierce, R. B., Pippin, M. R., Saiz-Lopez, A., Spurr, R. J. D.,  
1009 Szykman, J. J., Torres, O., Veeffkind, J. P., Veihelmann, B., Wang, H., Wang, J., and Chance, K.:  
1010 Tropospheric emissions: Monitoring of pollution (TEMPO), Journal of Quantitative  
1011 Spectroscopy and Radiative Transfer, 186, 17–39, <https://doi.org/10.1016/j.jqsrt.2016.05.008>,  
1012 2017.  
1013